Experimental Investigation of Passive Alternating Flow Heating Strategies for PEMFC Cold Start

El Ahmadi Mortada[a], Bégot Sylvie[a], Harel Fabien[b], Layes Guillaume[a], Lepiller Valérie[a]

(a) Université Marie et Louis Pasteur, CNRS, Institut FEMTO-ST, FCLAB, F-90000 Belfort, France

(b) Univ Eiffel, Univ Lyon, ENTPE, LICIT-ECO7, F-69675 Lyon, France

Highlights

- Experimental assessment of PEMFC cold-start behavior using a 3-cell thermal-emulation setup
- Alternating flow yields +32.3 °C in 85 s with horizontal and vertical uniformity below 3 °C and 1 °C, respectively.
- Identification of the limitations of conventional sub-zero PEMFC heating strategies
- Analysis of velocity and reciprocating-period effects on key thermal-performance metrics
- Proposal of an adaptive alternating-flow strategy enabling rapid heating while maintaining acceptable inter-cell temperature differences

Keywords

PEMFC stack, Passive cold start strategy, Alternating flow, Heat management

Nomenclature

Cp_{stack} $[\frac{J}{kgK}]$: Stack specific heat capacity

$C_p[\frac{J}{kgK}]$: Fluid specific heat capacity

$DC[\%]$: Duty cycle

$E_{elec}[J]$: Energy produced by the heating pads

$E_{stack}[J]$: Energy absorbed by the stack

$E_{cool}[J]$: Energy transferred by forced convection

$E_{surro}[J]$: Energy transferred by natural convection

h $[\frac{W}{m^2K}]$: Convective heat exchange coefficient

m_{stack} $[kg]$: Stack mass

Nu : Nusselt Number

PEMFC: Proton Exchange Membrane Fuel Cell

$P[s]$: Period

$Pow[W]$: Heating pads Power

Q_{nat} $[W]$: Natural convection heat transfer rate

$Q_v[\frac{L}{min}]$: Volumetric flow rate

$Qv_{dir}[\frac{L}{min}]$: Direct flow rate

$Qv_{rev}[\frac{L}{min}]$: Reverse flow rate

Ra: Rayleigh Number

$SR[\%]$: Stop Ratio

T [°C]: Temperature

$Ti[°C]$: Initial temperature

$T_A[°C]$: Temperature of Cell A

$T_M[°C]$: Temperature of Cell M

$T_K[°C]$: Temperature of Cell K

$TA_{in}[°C]$: Inlet temperature of Cell A

$TA_{out}[°C]$: Outlet temperature of Cell A

$TK_{in}[°C]$: Inlet temperature of Cell K

$TK_{out}[°C]$: Outlet temperature of Cell K

$TM_{in}[°C]$: Inlet temperature of Cell M

$TM_{out}[°C]$: Outlet temperature of Cell M

$TE_{in}[°C]$: Inlet temperature of Cell E

$TE_{out}[°C]$: Outlet temperature of Cell E

$TFC_{in}[°C]$: Inlet temperature of the stack

$TFC_{out}[°C]$: Outlet temperature of the stack

$t\ [s]$: Time

$\gamma[°C]$: Mean Temperature Increase

$\sigma[°C]$: Stack Temperature homogeneity

$\delta[°C]$: Cell Temperature homogeneity

$\Delta P[mbar]$: Pressure drop between inlet and outlet of the fuel cell

$\Delta t_{heating}\ [s]$: Heating duration

$\Delta T_{stack}[°C]$: Stack Temperature Rise

$\Delta T_{A,in/out}\ [°C]$: Cell A temperature difference between inlet and outlet inlet and outlet

$\Delta T_{M,in/out}[°C]$: Cell M temperature difference between inlet and outlet inlet and outlet

$\Delta T_{K,in/out}[°C]$: Cell K temperature difference between inlet and outlet inlet and outlet

$\Delta T_{A}[°C]$: Cell A temperature rise

$\Delta T_{M}[°C]$: Cell M temperature rise

$\Delta T_{K}[°C]$: Cell K temperature rise

$TFC_{in}[°C]$: External surfaces of the inlet tubes

$TFC_{out}[°C]$: External surfaces of the outlet tubes

$T_{S,A}[°C]$: External surface temperature of the clamping plates on the anode side

$T_{S,K}[°C]$: External surface temperature of the clamping plates on the cathode side

ABSTRACT

Passive cold start remains a major challenge to Proton Exchange Membrane Fuel Cells (PEMFCs), with thermal imbalance during warm-up being a key challenge. Uneven temperatures can cause startup failure and long-term degradation. This study experimentally evaluates a new passive heating strategy using alternating coolant flow to improve thermal management. Experiments are conducted using a 3-cell thermal-emulation stack (100 cm^2 per cell, ≈230 W thermal power), designed to replicate the edge and central-cell thermal behavior of real PEMFC stacks at –10 °C. The proposed method relies on alternating-flow operation, in which the coolant periodically reverses direction inside the cooling channels, enhancing heat retention and redistribution. This configuration is systematically compared with conventional no-flow (no coolant circulation) and unidirectional-flow (constant flow direction) using key thermal metrics, including temperature rise, vertical and horizontal uniformity, and forced-convection losses. Results show that the no-flow configuration enables rapid heating but induces significant inter-cell temperature differences, resulting in poor horizontal uniformity. Unidirectional configuration provides better horizontal uniformity but limits heating capability and leads to vertical temperature stratification at the cell level due to convective heat removal. The proposed alternating-flow strategy outperforms both reference cases, achieving a 32.3 °C temperature rise in 85 s, reducing vertical gradients by 90 %, and decreasing inter-cell temperature dispersion by more than 63 %. Under these conditions, the active surface exceeds 0 °C, enabling safe cold start. An adaptive strategy is proposed, dynamically switching flow modes based on internal thermal monitoring. This scalable approach offers a promising passive solution for cold-start management in PEMFCs.

1. Introduction:

Proton Exchange Membrane Fuel Cells (PEMFCs) are electrochemical devices that convert hydrogen and oxygen into electricity, heat, and water. While they are considered key elements of the hydrogen economy [1], their reliable operation at sub-zero temperatures remains a major barrier to large-scale their deployment. When the fuel cell temperature drops below 0 °C, the water produced at the cathode catalyst layer freezes, which can block oxygen transport to the cathode side during PEMFC start-up. These phenomena lead to a voltage drop in the PEMFC, compromising cold start capability and accelerating PEMFC degradation [2] [3].

The cold start of a PEMFC involves a strong interdependence between the transport of water produced by the electrochemical reaction and the heat required to warm up the fuel cell. If the produced water is not effectively removed and the generated heat is insufficient to raise the cell temperature above the freezing point, ice will form in the cathode catalyst layer (CCL). This can result in cold start failure and accelerate the degradation of PEMFC components [4]. Cold start requirements for fuel cell vehicles have been defined internationally. In the U.S., DOE targets require 50% rated power at –20 °C within 30 s, autonomous start-up at –30 °C, and assisted start-up at –40 °C [5]. Vehicles such as the Toyota MIRAI and Hyundai NEXO have already demonstrated –30 °C starts, relying on optimized designs and advanced control [6]. A key challenge remains achieving a rapid and uniform temperature rise without external heating.

Oszcipok et al. [7] and Hou et al. [5] demonstrated that ice accumulation occurs primarily on the cathode side. It can obstruct oxygen flow and consequently reduce the cathodic oxidation reaction. This freezing leads to a significant voltage drop and increases the cell's electrical resistance, ultimately preventing the fuel cell from starting up [8]. Liang et al. [9] analyzed ice formation during PEMFC cold starts using in situ techniques and showed that long-term icing in the catalyst layer or gas diffusion layer leads to severe irreversible degradation. Their degradation map highlights that rapid and uniform heating is essential to suppress ice formation and ensure durable cold starts. Lv et al. [10] conducted a comprehensive experimental study on a 110 kW, 370-cell PEMFC stack during cold start at –30 °C, focusing on voltage uniformity, the so-called "bucket effect" whereby the weakest single cell dictates stack performance. Their results showed strong end-plate effects: side cells near the positive electrode consistently underperformed

due to enhanced heat loss, while blocking coolant chambers of unipolar and dummy cells significantly improved voltage consistency. Their study also highlighted the influence of operating parameters such as the coolant flow rate. It improves temperature and voltage uniformity up to a point, but excessive flow removes too much heat and causes startup failure. Lin et al. [11] investigated the cold start behavior of a PEMFC stack under constant voltage mode and showed that the stack achieved rapid startup at −15 °C in 95 s, outperforming single-cell operation. Their results revealed strong spatial inhomogeneities: the middle cells exhibited the best cold start performance, while inlet-side cells suffered the most severe degradation. These findings highlight that internal behavior of the various cells differs during the cold start process, resulting in performance inhomogeneity. Wan et al. [12] investigated the impact of end plates on PEMFC performance during cold start, combining stack tests and a segmented single cell to mimic end-cell behavior. Their results showed that end cells consistently exhibited the lowest performance due to stronger heat losses, lower local temperatures, and accelerated ice blockage in the Membrane Electrode Assembly (MEA) or channels. Wang et al. [13] experimentally evaluated the rapid cold start-up performance of a 70 kW automotive PEMFC system without auxiliary PTC heating, analyzing control strategies, purging, and voltage distribution. At −30 °C, end-plate cells showed severe voltage drops and reverse polarity due to local freezing, despite the coolant outlet reaching 20 °C within 90 s. Shan et al. [14] developed a zero-dimensional model incorporating temperature effects, and their results revealed pronounced edge effects in the temperature distribution of a 10-cell stack. Lin et al. [15] reported that the evolution of peak current density and temperature differs between successful and failed starts, identifying the inlet and middle regions as critical. Ren et al. [16] used printed circuit board technology to investigate internal current density and temperature under different flow field designs. Their results demonstrated that flow field configuration plays a crucial role in improving cold-start capability and durability. Furthermore, the non-uniform distribution of physical fields can lead to localized or partial icing within individual cells, even during an otherwise successful cold start [17]. Yang et al. [18] demonstrated that, after 30 cold-start failures, the downstream region experienced the most severe degradation, while only mild damage was observed in the middle and upstream regions. They further identified freezing-induced crack formation, platinum particle growth, and ionomer agglomeration in the catalyst layer as the main mechanisms responsible for freeze damage. Yang et al. [19] investigated voltage consistency during the cold start of a 7-kW, 46-cell PEMFC stack. Their results revealed a pronounced end-plate effect, with voltage consistency deteriorating as the start-up temperature decreased. Zhong et al. [20] experimentally analyzed low-temperature consistency in a five-cell stack and found that Cell 1, located the nearest to the gas inlets, exhibited the most severe performance degradation after 20 freeze–thaw cycles.

Su et al. [21] provided a comprehensive review of liquid-cooling thermal management strategies for PEMFCs, with a focus on temperature regulation and cold start. They emphasized that severe temperature non-uniformity and voltage inconsistency often occur during PEMFC cold starts, threatening both performance and durability. They reviewed control-oriented solutions such as stepwise current profiles, closed-loop cold start control, and purge strategies, typically combined with auxiliary heaters. While these methods improve start-up reliability, they rely on active control and external energy input. Amamou et al. [22] also developed a cold start adaptation strategy, which combines online parameter identification with a semi-empirical model. It aims to manage uncertainties in operating conditions and track the optimal operating point in real time. Li et al. [23] used a 3D multiphase model to assess coolant-, air-, and combined heating at −20 °C. Coolant heating was most effective, while the air + coolant strategy reduced ice fraction by 7.7% and shortened start-up by 2 s. However; the study lacked experimental validation and remained dependent on active heating.

Therefore, to ensure a successful start-up, the cell temperature must rise above the freezing point before all the pores of the CCL become clogged with ice. To achieve this, various solutions exist to enable rapid stack heating. A. Amamou et al. [24] presented them in a comparative study. The solutions are divided into two categories: passive strategies, in which the heat source is the fuel cell itself, and active (or external) strategies, which rely on external auxiliaries -, such as preheaters, heating elements, batteries, etc.- added to the stack to raise its temperature

Recently, alternating (or reciprocating) flows have emerged as a promising solution to the issue of temperature inhomogeneity in electrochemical systems. By definition, a reciprocating flow is a flow that

periodically reverses its direction [25] [26], typically using a simple flip-door valve mechanism [27]. Their application to battery thermal management - where BTMS targets is to keep the maximum temperature between 10 and 50 °C [28] and the temperature difference below 5 °C [29] - has been extensively investigated through many studies. Z. Jiang et al. [30] showed that a heat-pipe + mist-air cooling system reduced the maximum battery temperature by 20% and thermal gradients by 60% versus unidirectional cooling. W. Zeng et al. [31] tested a numerically simulated liquid BTMS with alternating flow, which reduced the thermal gradient by 55.3%, the maximum temperature by 3.3%, and energy consumption by 15.6%. K. Yu rt al. [32] introduced a thermal control model with adjustable valves, reducing the maximum temperature by 4.63 K and the temperature difference by 7.68 K. He and Ma [33] used a reduced-order model (ROM) to limit the thermal gradient from 4.2 °C to 1 °C, reducing air flow rate by 38.5%. Park and Jaura [34] showed that an alternation period of 30 seconds decreased the thermal gradient from 4.73 °C to 0.58 °C and reduced the maximum temperature from 34.7 °C to 33.1 °C. Ping et al. [35] optimized the cooling of LiB modules through CFD simulations using alternating air flow, improving heat dissipation. Wang et al. [36] designed a dual-channel system for a LiB module, lowering the temperature from 69.8 °C to 55 °C at a 1C discharge rate, achieving 73% efficiency thanks to the alternating airflow. Alam et al. [37] evaluated the Reciprocating-Mechanism Driven Heat Loop (RMDHL), showing its potential for high heat flux electronics cooling.

In the case of PEMFCs, Bégot et al. [38] proposed a novel PEMFC cooling circuit enabling alternating flow strategies, which accelerate temperature rise by trapping heated fluid while maintaining acceptable gradients. The patented system [39] can be integrated into vehicle applications. H. Shen et al. [40] numerically studied a five-cell PEMFC with straight channels under four cooling modes: unidirectional (A), interlayer reverse (B), adjacent reverse (C), and alternating (D). Modes C and D reduced temperature differences by 4.3 K and 3.2 K and increased power density by 23% and 20.6%, respectively.

Stack & Conditions	Heating Strategy	Method	Active/ Passive	Key Findings
5-cell, 50 cm² (–5°C to –25°C) [11]	Constant voltage cold start	Experimental (PCB-based)	Passive	Rapid start at –15 °C in 95 s. Voltage inhomogeneity observed; middle cell performs best.
10-cell and single-cell (–10 °C to –30 °C) [12]	Potentiostatic start	Experimental (segmented cell to simulate end effects)	Passive	Single-cell fails at –10 °C; end cells show lowest voltage due to heat loss.
12-cell, 271 cm² (–10 °C to –30 °C) [41]	Constant current + voltage protection	Experimental	Passive	Reduced ramp extends startup time but improves stability. Below –20 °C, thermal imbalance increases.
290-cell, 330 cm², 70 kW (–20 °C to –30 °C) [13]	Stepwise increase to 0.8 A/cm² (20 A/s)	Experimental	Passive	50% power reached in 25 s at –20 °C; reverse polarity in end cells at –30 °C.
46-cell, 7 kW, 50 cm² (–10 °C to –40 °C) [42]	Passive self-heating + coolant heating	Experimental	Combined	Startup in 30–57 s at –20 °C and –25 °C. Combined strategy improves consistency.
370-cell, 298 cm², 110 kW (–30 °C) [10]	Stepwise current to 105 A in 35 s, then hold	Experimental	Passive	Voltage drops with temperature; severe end-cell degradation at –30 °C.
80 kW, 300 cm² (–30 °C) [42]	PCM + PTC with self-start	Numerical	Combined	PTC-PCM reduces cold-start time and energy use by ~19%.
3D flow model (–20 °C) [23]	Air vs. coolant-assisted vs. combined	Numerical	Active	Coolant heating improves startup; combining with air cuts ice by 7.7% and startup time by 2 s.

335-cell, 190 cm², 50 kW (–5 °C to –25 °C) [43]	Waste heat recovery + PCM + PTC	Numerical	Active	Cuts PTC use time by 73% and power by 45%; reuses heat for preheating.
370-cell (–20 °C) [44]	PCM into TMS for post-shutdown temp hold	Numerical	Active	Maintains stack > 0 °C for 63 h at -20 °C environment.

Table 1: Summary of reported PEMFC cold-start strategies, operating conditions, and main outcomes.

The Table 1 summarizes key experimental and numerical studies addressing PEMFC cold starts, highlighting the type of heating strategy (active, passive, or combined), methodology, test conditions, and observed performance. While active strategies using external heaters—such as Positive Temperature Coefficient (PTC) elements or Phase Change Materials (PCM)—or advanced control algorithms can achieve rapid startup [44] [19] [43], they inevitably increase energy consumption, hardware complexity, and integration costs [45] [21]. In contrast, passive approaches avoid auxiliary power but still face a major limitation: thermal non-uniformity persists even during successful cold starts [19], with end cells typically colder than central ones [11] [13], and significant inlet–outlet gradients within each cell. This recurring imbalance is observed in both small-scale and large-scale stacks [11] [12] [13], highlighting the need for improved passive thermal redistribution techniques.

Among potential solutions, alternating coolant flows have shown promise for enhancing heat redistribution and temperature uniformity. Yet, despite encouraging simulation and conceptual studies [38] [40], a comprehensive experimental evaluation of liquid-based alternating flow heating strategies—specifically under sub-zero conditions—remains lacking. This work addresses that gap by experimentally investigating alternating flow strategies using a dedicated PEMFC thermal emulator under controlled sub-freezing conditions.

Figure 1 outlines the methodological framework of the study. The approach aims to address the cold-start thermal imbalance in PEMFCs by developing a passive heating strategy based on alternating coolant flow. A dedicated thermal emulator, replicating realistic stack boundary conditions, is employed to isolate heat redistribution phenomena independently of electrochemical processes. This approach provides new insights that are difficult to obtain in real stacks, where reactant leakage and ice formation pose safety risks and measurement challenges. Several heating configurations are tested, including conventional modes (no-flow, unidirectional flow) and newly proposed alternating flow strategies. Key thermal performance indicators—temperature rise rate, inter-cell uniformity, and convective heat losses—are systematically quantified. A comparative analysis is conducted to evaluate each configuration's effectiveness, leading to the development of an adaptive flow control strategy. The study concludes with a synthesis of the results, highlighting the potential of alternating flow as a robust, low-cost, and scalable passive solution for cold-start thermal management in PEMFC systems.

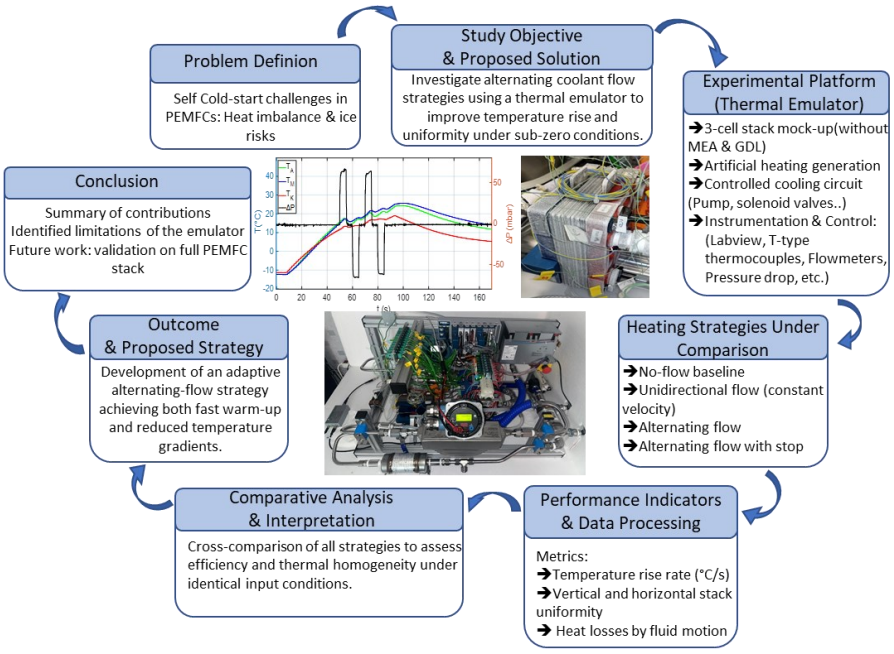

Figure 1: Methodological framework diagram

2. Materials and methods:

2.1 Experiment test bench and experimental design:

This study builds upon an experimental fluidic test bench previously used in an earlier investigation [38]. The test bench Figure 2 (a) has been developed and adapted to meet the requirements of the present study. In the following sections, we describe the experimental setup and all the new developments made to the bench. As indicated in the Schematic diagram Figure 2 (b), the fluidic bench consists of a proton exchange membrane fuel cell (PEMFC) stack whose electrochemical core components (membrane electrode assembly and gas diffusion layers) have been removed and replaced by heating pads, a pump that circulates the coolant through the loop, two heat exchangers (HEX 1 and HEX 2) in series (each connected to a chiller), two 3-way solenoid valves responsible for reversing the flow direction, and the associated instrumentation. The main actuators in the fluid control circuit (pump, solenoid valves) are sourced from the automotive industry, which allows us to assess their suitability for the constraints of our study and also to anticipate their possible future integration into an onboard technical solution.

The measurement and control of the test bench are performed using a National Instruments CompactDAQ system and a dedicated application developed with LabVIEW software Figure 2 (c).

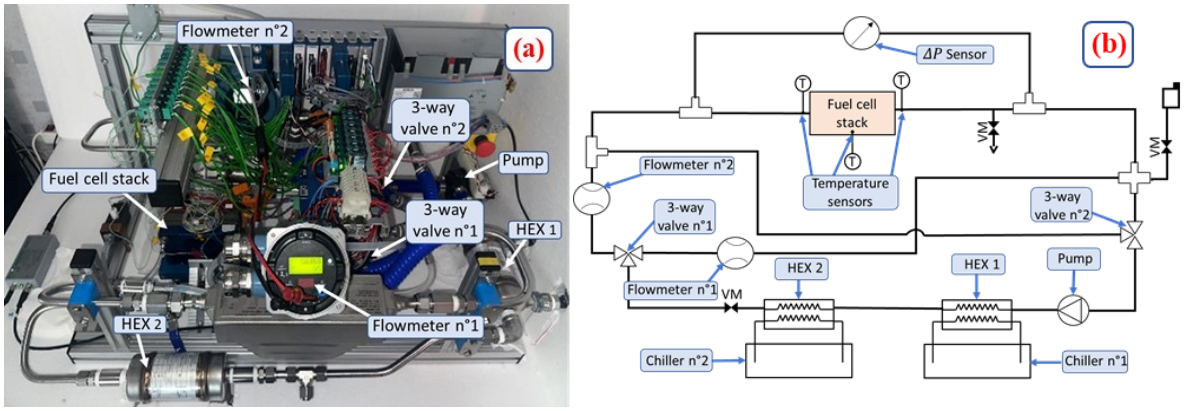

Figure 2: a) Test bench; b) Complete setup with instrumentation; c) Control panel of the software

The fuel cell used in this study (Figure 3(a)) is based on a commercially available liquid-cooled model manufactured by ZSW. The assembly consists of three cells (A, M and K) with dimensions of 10 x 10 cm^2 (Figure 3 (b)). Each cell comprises a heating pad and a bipolar plate (cooling plates). The cells are designated as follows:

- Cell A: the cell on the anode side,
- Cell M: the central cell,
- Cell K: the cell on the cathode side.

A fourth cooling plate, designated E, is added to provide additional cooling on the anode side. Current collector plates and end plates enclose the three cells. This is standard stack design. The 3-cell thermal emulator used in this study was specifically designed to reproduce the key thermal phenomena occurring in larger systems. such as edge effects, inter-cell gradients, and heat redistribution across coolant channels. Previous studies have demonstrated that such thermal behaviors can be reliably observed at small scale when boundary conditions and flow geometry are representative [11]. Furthermore, by excluding electrochemical reactions, the emulator isolates the intrinsic thermal response of the stack, allowing safe and repeatable analysis of heating strategies under sub-zero conditions.

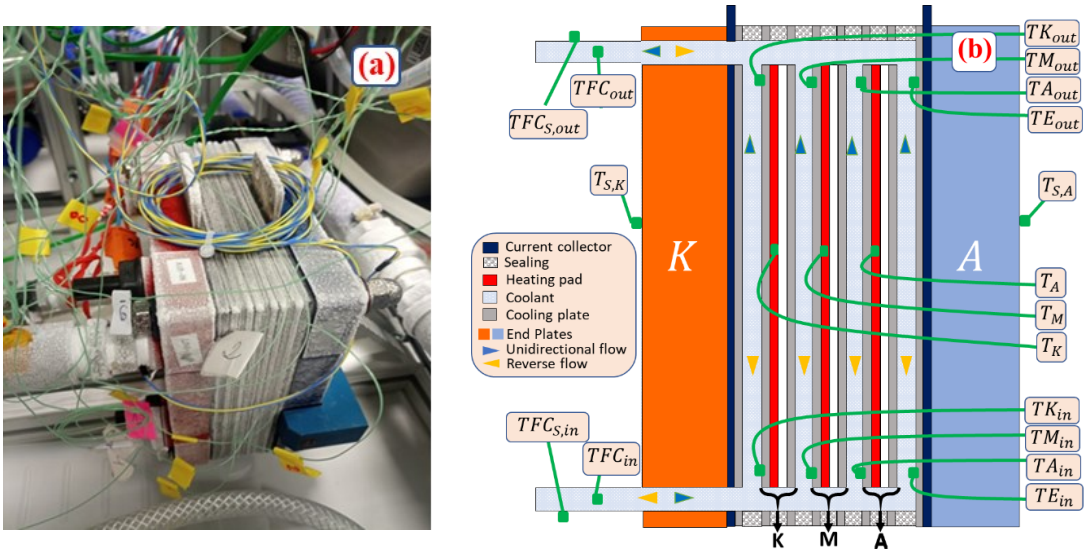

Figure 3: a) fuel cell under frozen conditions at –10 °C; b) Stack assembly with temperature sensor positions

Three heating pads with dimensions of 10 x 10 cm^2 are inserted on the cathode side of each bipolar plate to reproduce the heat generation of the fuel cell during regular operation. The power supplied to the heating pads is measured using a Hall effect current sensor and a voltage measurement. The thermal power density achieved in this study is of 0.72 W/cm^2, which is comparable to the thermal power density observed in real PEM fuel cell operation. In fact, during successful cold starts, thermal power densities between 0.5 W/cm^2 and 0.9 W/cm^2 have been reported [11]. The maximum power output of the three cells is approximately 233 W. The heating power delivered by the pads is independently adjustable for each cell. Each pad can supply its full nominal power but operates in a discontinuous (pulsed) mode, such that the time-integrated

energy corresponds to the desired power. This configuration allows precise control of the applied heat flux. The contribution of the membrane electrode assembly and gas diffusion layers to the total thermal capacity of the stack is considered as negligible compared to that of the coolant and bipolar plates [48].

The cooling fluid used is designated as "Glysantin FC G 20-00/50." Ethylene glycol is the main chemical component of the mixture, with a concentration between 45% and 55%. The product remains liquid at very low temperatures, down to -38°C. Cooling to sub-zero temperatures is achieved using two heat exchangers in series, each connected to a chiller in a closed loop. Two CF40 chillers from Julabo were connected in series, each linked to a heat exchanger in a closed loop. This configuration enabled cooling of the stack to –10 °C under ambient laboratory conditions. The choice of –10 °C as the initial temperature is pragmatic, as it reflects in this study a representative cold-start scenario and provides a consistent reference point for comparing the performance of different strategies in improving the thermal behavior of the fuel cell stack.

Two Coriolis flowmeters measure the flow rate in the circuit with an accuracy of 0.2%. The first flowmeter measures the direct flow rate (Qv_{dir}) in the pump circuit, while the second measures the reverse flow rate (Qv_{rev}). With this flowmeter technology, the measurement is independent of temperature. The pressure difference (ΔP) between the inlet and outlet of the fuel cell cooling channel is measured by a Keller PD33X differential piezoelectric sensor, with an accuracy of 0.1%.

Temperature measurements are primarily located on the studied fuel cell, using several thermocouples of various sizes. A surface thermocouple with a diameter of 6.35 mm is attached at mid-height of each heating element. These sensors were calibrated in the laboratory, and their measurement uncertainty is estimated at ±0.5°C. The connecting wires are routed either through the unused gas circuit or the sealing plates for smaller diameter wires. The corresponding temperatures of the three heating pads are denoted as TA, TM, and TK. Laboratory-fabricated thermocouples with a wire diameter of 127 µm are inserted at the inlet and outlet of each cell's cooling channels and at the inlet and outlet of the additional cooling plate (E). Their measurement uncertainty is also estimated at ±0.5 °C. The designations are: $TA_{in}, TA_{out}, TK_{in}, TK_{out}, TM_{in}$ and TM_{out} for the inlet and outlet of cells A, M, and K respectively, and TE_{in}, TE_{out} for the additional cooling plate.

Two thermocouples (TFC_{in} and TFC_{out}) fabricated with a wire diameter of 127 µm, are also inserted directly into the coolant at the inlet and outlet of the fuel cell. Two additional thermocouples are affixed to the external surface of the inlet and outlet tubes ($TFC_{S,in}, TFC_{S,out}$). These sensors were also calibrated in the laboratory. On the external surfaces of the clamping plates, one thermocouple is positioned on the anode side and the other on the cathode side of the fuel cell ($T_{S,A}, T_{S,K}$). A type K thermocouple is placed outside the system to measure the handling room's ambient temperature ($Tamb$).
The Figure 4 illustrates the possible flow directions with our test bench. Configuration (a) is the default setup (unidirectional flow), while configuration (b) reverses the flow direction. A third configuration, (c), allows the stack to be bypassed using the first solenoid valve in configuration (b) and the second in configuration (a). In the pump, the fluid always flows in the same direction.

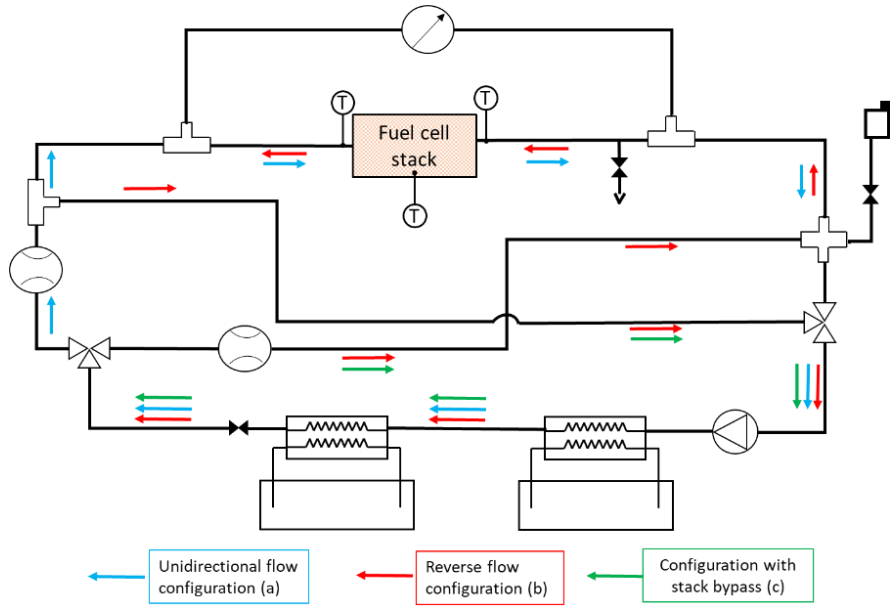

Figure 4: Possible flow configurations within the test bench

These three configurations allow us to define the five startup strategies studied in the experimental plan (Table 2), two conventional and two new ones. The first is when the pump is stopped, and there is no fluid circulation in the cooling loop; this strategy is called "S1." The second reference strategy is when the fluid flows unidirectionally through the stack, called "S2." The third strategy involves alternating the coolant flow through the stack with variable periods (P) and duty cycles (DC), meaning the amount of fluid moved through the stack during a complete period can be adjusted between the half-periods, referred to as "S3". The fourth proposed strategy is based on reversing the fluid direction through the stack. After each movement in a given direction, a stop phase, called the Stop Ratio (SR), is introduced, during which the fluid flow through the stack is paused; this strategy is referred to as "S4". The last strategy denoted "S5" is an adaptive strategy combining S1 and S4 strategies during the startup.

Ti	Strategy	Qv[L/min]	P [s]	DC	SR
$-10°C$	S1				
	S2	0.1			
	S2	0.3			
	S2	0.5			
	S3	0.5	16	50%	
	S4	0.5	16	50%	50%
	S5	0.5	16	50%	50%

Table 2: Experimental design

2.2 Performance assessment:

Four criteria are used to compare the strategies (Table 3). The first, "γ", is the average temperature rise of the three stack cells. The second, "σ ", measures horizontal temperature uniformity across the stack. It is the standard deviation of the temperature variation of the cells. The third, "δ", assesses vertical uniformity along cell height. It is the maximum value of the average temperature difference of the fluid measured between the inlet and the outlet of the three cells. The fourth indicator, "E_{cool}", is the energy carried by the fluid flow, measured at the stack's inlet and outlet. This allows us to estimate the heat transfer to the fluid during startup. The calculation is performed iteratively for each measurement point from the temperature difference between the inlet and outlet of the stack and multiplied by the fluid flow rate (Qv). This method provides dynamic tracking of the energy transferred by forced convection to the coolant within the stack.

Performance criterion	Description	Formula	Units
Mean temperature increase γ	The temperature rise of cells A, M, and K from the initial temperature to the temperature reached after 85 seconds of heating is evaluated. The average temperature rise of the three cells is also calculated.	$\Delta T_A = T_{A(t=t0+85s)} - T_{A(t=t0)}$ $\Delta T_M = T_{M(t=t0+85s)} - T_{M(t=t0)}$ $\Delta T_K = T_{K(t=t0+85s)} - T_{K(t=t0)}$ $\gamma = Mean(\Delta T_A; \Delta T_M; \Delta T_K)$	°C
Temperature homogeneity within the stack σ	The standard deviation of the temperature rise in the three cells estimates the temperature uniformity along the stack (horizontal uniformity).	$\sigma = Std(\Delta T_A; \Delta T_M; \Delta T_K)$	°C
Temperature homogeneity at the cell level δ	The temperature homogeneity at the cell level is evaluated by calculating the maximum value of the average temperature difference of the fluid measured between the inlet and the outlet of the three cells (vertical uniformity).	$\Delta T_{A,in/out} = Mean\ (T_{A,out} - T_{A,in}\ )$ $\Delta T_{M,in/out} = Mean\ (T_{M,out} - T_{M,in})$ $\Delta T_{K,in/out} = Mean\ (T_{K,out} - T_{K,in}\ )$ $from\ t = t0\ to\ t = t0 + 85s)$ $\delta = Max(\ \Delta T_{A,in/out}\ ; \Delta T_{M,in/out}\ ; \Delta T_{K,in/out})$	°C
Convective energy transfer E_{cool}	The energy transported by the fluid motion through forced convection is quantified at the inlet and outlet of the stack in order to evaluate the heat transfer induced by the heating strategy.	$E_{cool} = \sum_{i=t0}^{t0+85s} \rho Q v_i C_p (T_{out,i} - T_{in,i})(t_i - t_{i-1})$; $(from\ t = t0\ to\ t = t0 + 85s)$	J

Table 3: Key performance indicators

The energy balance applied to our system during the startup phase is described by (Eq. 1). The heat source in our system is the fuel cell itself (Eq. 2), which generates thermal power via heating pads ($E_{elec} = 19.8kJ$). Since the ambient temperature of the room surrounds the stack, natural convection (E_{surro}) occurs due to the temperature difference between the stack and the environment (Eq. 3). It tends to heat the fuel cell. The heat transfer by natural convection is computed using (Eq. 4) where "Ra" denotes the Rayleigh number and "Nu" the Nusselt number. It leads to a Nusselt number of 15.5. Heat transferred by natural convection (E_{surro}) is about 1.2 kJ. The thermal energy supplied to the stack during the heating phase is estimated to be 20.2 kJ taking considering the natural convection. The energy from the surroundings (E_{surro}) is less than 10% of the electric energy supplied.

$$E_{elec} = E_{stack} + E_{cool} - E_{surro} \text{ (Eq. 1)}$$

$$E_{elec} = P * \Delta t_{heating}\ (from\ t = t0\ to\ t = t0 + 85s) \text{(Eq. 2)}$$

$$E_{surro} = Q_{nat}\ * \Delta t_{heating}\ (from\ t = t0\ to\ t = t0 + 85s) \text{ (Eq. 3)}$$

$$Nu = 0.59 * Ra^{0.25} \text{ (Eq. 4)}$$

$$E_{stack} = m_{stack}\ .\ Cp_{stack}\ .\ \Delta T_{stack} \text{ (Eq. 5)}$$

Ra	Nu	$h\ [W/m^2K]$	$Q_{nat}\ [W]$	E_{surro} [kJ]
4.8×10^5	15.5	7.6	13.7	1.2

Table 4:Quantification of natural convection

Thermal energy generated in the fuel cell is transferred through two main paths: E_{stack} represents the energy used by the stack to raise its temperature (Eq. 9). It depends on the stack's materials density and specific heat capacities. E_{cool} is the energy transferred through forced convection in the cooling circuit.

Assuming E_{surro} and E_{elec} stay constant during heating, E_{stack} only depends on E_{cool}. Heating strategies should minimize coolant losses to raise the stack temperature while keeping thermal uniformity.

2.3 Startup protocol:

The startup protocol is as follows:

- Step 1: Start the pump in unidirectional mode
- Step 2: Activate the two chillers and wait for reaching a stable temperature of -10°C inside the fuel cell (around 2 hours)
- Step 3: Select the flow rate (Software flow rate regulation)
- Step 4: Start alternating fluid modes if applicable (solenoid valves software timing control)
- Step 5: Supply the one or all the heating elements for the chosen duration
- Step 6: Cooling

The entire sequence is controlled automatically by custom-developed software, ensuring that all cold-start tests follow the exact same steps (Figure 2 (c)). The duration of the heating phase is 85 s, similar to the duration used by Yang et al. [19].

3. Experimental results and discussion:

This section presents and discusses the experimental results through the following key subsections:

- Comparative analysis of four heating strategies and their respective thermal performances;
- Parametric investigation of the effects of flow velocity and reversal period;
- Application case highlighting the thermal optimization of peripheral cells using alternating flow;
- Development of an adaptive flow control strategy (S5) for improved cold-start management.

3.1 Comparative Analysis of Heating Strategies:

The analysis begins with a comparison of standard heating strategies used in PEMFC cold start, highlighting their respective strengths and limitations. These serve as a baseline for evaluating alternative flow configurations. Subsequently, alternating-flow strategies are examined, with particular attention to the underlying heat transfer mechanisms.

3.1.1 Reference tests, no-flow strategy: S1

In the first instance, the pump is stopped. As a result, the cooling liquid did not circulate in the stack ($Qv_{dir} = Qv_{rev} = 0$). Rise in temperature of the heating pads TA, TM, TK is given in Figure 5 (a). Constant power applied is 233 W for 85 seconds as required.

All temperatures measured by the instrumented thermocouples at the inlet and the outlet of each cooling plate, as well as in inlet and outlet of the fuel cell ($TA_{in}, TA_{out}, TK_{in}, TK_{out}, TM_{in}, TM_{out}$, TE_{in}, TE_{out}, TFC_{in}, TFC_{out}) are combined in the following Figure 5(b).

The results indicate a noticeable temperature increase across the three heating pads. The central cell (M) reaches the highest temperature of 38.1 °C, while cell K remains the coldest, with a maximum temperature of 25.3 °C. Cell A exhibits a similar behavior to cell M, with slight variations. The average temperature increase (γ) of the heating pads is 44.2°C.

In this case, heat transfer is limited to conduction and natural convection, reducing heat dissipation. Conversely, the outlet temperature of the fuel cell stack, TFC_{out} is higher than the inlet temperature, TFC_{in}. This behavior is likely attributed to natural convection within the stack, as the inlet is located at the bottom and the outlet at the top. Moreover, heat exchange from the environment tends to increase the temperature. In the additional cooling plate E, both inlet and outlet temperatures, TE_{in} and TE_{out} , increase due to heat transfer by conduction from the adjacent cell A.

The central cell M is, in fact, better insulated from the ambient temperature than the other cells (Figure 3 (b)). The thermal resistance between the ambient air and the heating plate is lower on the cathodic side

(cell K) than on the anodic side (cell A) due to the presence of the additional cooling plate (E). As a result, cell A has a higher temperature.

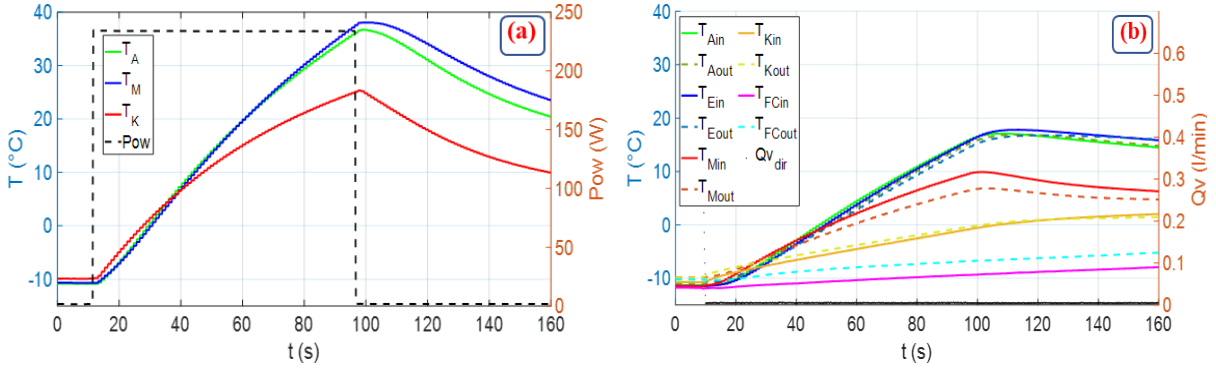

Figure 5: No-flow strategy "S1": (a) Heating pad temperature, applied power; (b) Cooling plates channel temperatures, flow rate

The S1 strategy achieved a significant temperature rise ($\gamma = 44.2\ °C$) within 85s but results in considerable thermal non-uniformity across the stack ($\sigma = 7°C$) . While this approach is practical for rapid heating, under freezing conditions and for stacks with a larger number of cells, the temperature gradient is likely to increase further. This is because the central cells are more thermally insulated and thus heat up primarily, whereas the edge cells dissipate heat more easily with the environment.

In real operating conditions, such overheating can lead to the rapid evaporation of water from the membrane [49] [46], causing a drastic increase in membrane resistance and, consequently, a voltage drop. This non-uniform temperature distribution results in heterogeneous degradation across the active surfaces of the cells. This reference test highlights the necessity of implementing heat transfer fluid circulation during the cold start phase to ensure thermal management and stack protection.

3.1.2 Reference tests, unidirectional flow strategy: S2

The second reference (S2) strategy corresponds to a unidirectional cooling fluid flow through the fuel cell stack (from bottom to top), replicating the standard flow direction typically used in PEMFC cooling loops. Three flow rate values were selected: 0.1 L/min, representing the minimum flow rate achievable within our experimental setup, 0.5 L/min, corresponding to the maximum allowable flow rate for the fuel cell mock-up; and an intermediate value of 0.3 L/min.

For each startup at a given flow rate, two plots present the recorded data during the startup phase for each flow rate. The first plot (Figure 6 (a), (c), (e)) shows the temperature rise of the heating pads (TA, TM, TK) along with the applied power (Pow). The second plot (Figure 6 (b), (d), (f)) displays the inlet and outlet temperatures of each cell ($TA_{in}, TA_{out}, TK_{in}, TK_{out}, TM_{in}, TM_{out}$), the auxiliary plate ($TE_{in}$, TE_{out}), and the fuel cell stack (TFC_{in}, TFC_{out}), as well as the volumetric flow rate corresponding to the fluid circulation: Qv_{DIR}. In this configuration, Qv_{REV} remains zero, as the flow is strictly unidirectional through the stack.

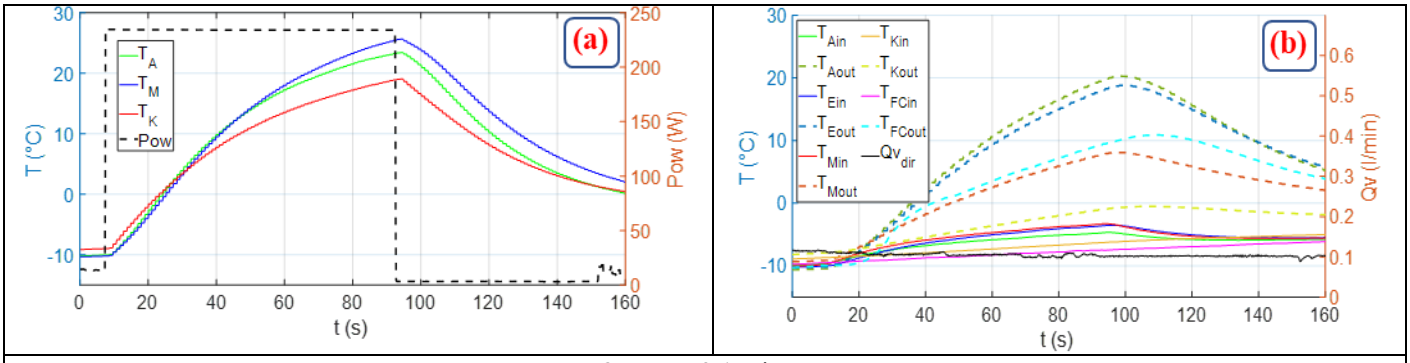

$Qv_{DIR} = 0.1\ L/min$

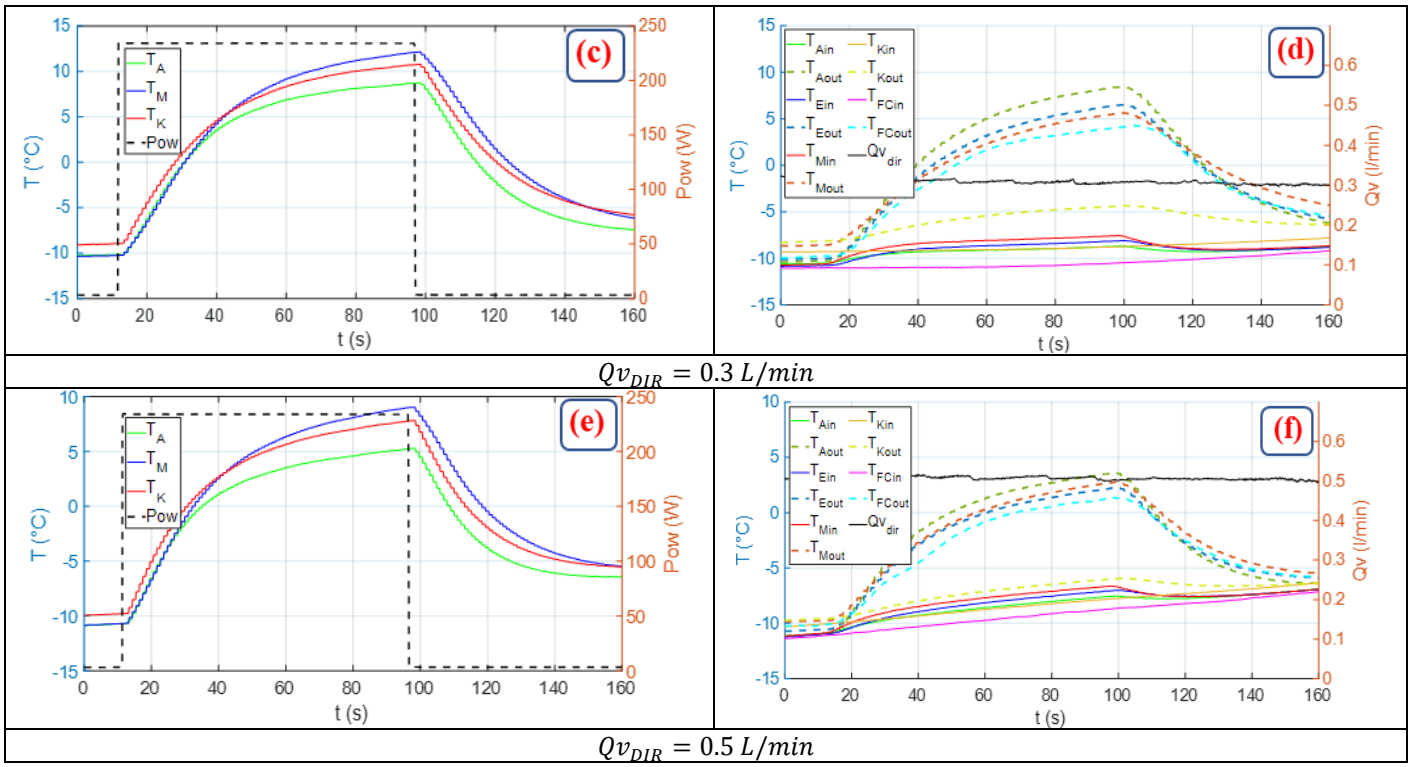

Figure 6: Unidirectional flow strategy "S2"at three different flowrates: (a) (c) (e) Heating pad temperature, applied power; (b) (d) (f) Cooling plates channel temperatures, Direct flow rate

Heating pad temperatures rise rapidly above freezing, reaching average temperatures of 22.7°C, 10.6°C, and 7.4°C, at the end of the heating phase for flow rates of 0.1 L/min, 0.3 L/min, and 0.5 L/min, respectively. The results of start-up tests with the S2 strategy show a significant temperature difference at the cell inlets and outlets δ, between 9.8°C and 6.3°C, depending on flow rate. At the end of heating, all temperatures measured at the inlets of the three cells (A, M, and K) are below 0°C. This highlights that these areas are probably favorable to the formation of ice. This phenomenon can pose significant problems under actual operating conditions. In our experimental mock-up, heat is generated homogeneously across the entire active surface, simplifying analysis. However, under real operating conditions, heat distribution is uneven, increasing the likelihood of ice formation at critical points. Increasing the flow rate improves temperature uniformity between cells, resulting in a more even thermal distribution. Indeed, horizontal uniformity σ is reduced by up to 2.4°*C* for the maximum flow rate strategy compared to S1 (σ=7°C). However, this improvement comes at the expense of overall temperature rise in the stack, which decreases with higher flow rates. Figure 7 shows that heat transfer to the fluid tends to increase with flow rate as expected.

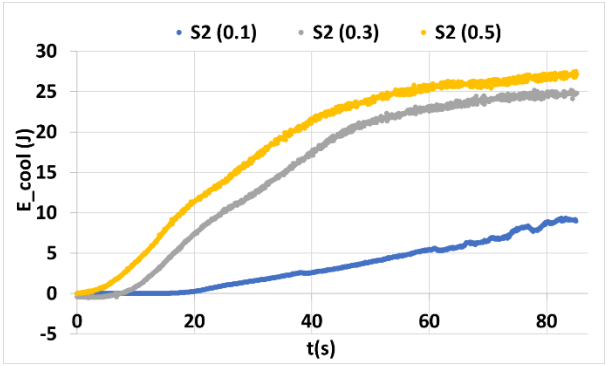

Figure 7: Energy transported by fluid flow under S2 strategy

Examining the state of the fuel cell after start-up (Figure 8) reveals that frost persists on the lower part of the stack, corresponding to the cell inlet regions. This observation is particularly critical, as it highlights

zones of intense cooling where the heat generated is insufficient to counterbalance thermal losses. Furthermore, the stack's last cooling plate (E), located on the anode side, remains covered with ice. As a result, the cell associated with this plate (A) is consistently the coldest in the stack.

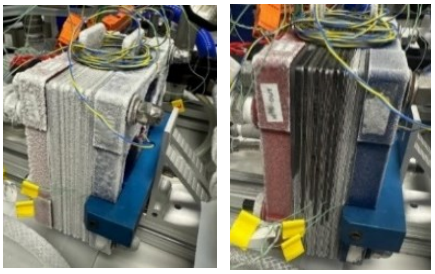

Figure 8: Photos of the stack before and after startup at -10°C

3.1.3 Alternating flow strategy: S3

The fluidic bench was developed to generate an alternating movement of coolant through the stack, with variable duty cycles. It means that the amount of fluid moved through the stack over a whole period can be adjusted between half-periods, A 50% duty cycle was selected, as the quasi-symmetric stack configuration provided optimal vertical homogeneity. The 2nd Coriolis flowmeter enables us to measure the flow rate in the opposite direction (Qv_{rev}) . Below (Figure 9(a)) is a recording of the flowmeter signals and the pressure variation signal between the inlet and outlet of the stack during one cycle of a cold start with strategy S3. The liquid flows at 0.5 L/min —chosen to allow direct comparison with unidirectional strategies using the same flow rate. Flow reversal occurred every 8 s thanks to the 2 3-way solenoid valves. The change in flow direction, when the solenoid valve is triggered, causes significant variations in the signals of these sensors. The pressure sensor indicates a sharp drop and stabilizes at a negative value, confirming a change in flow direction.

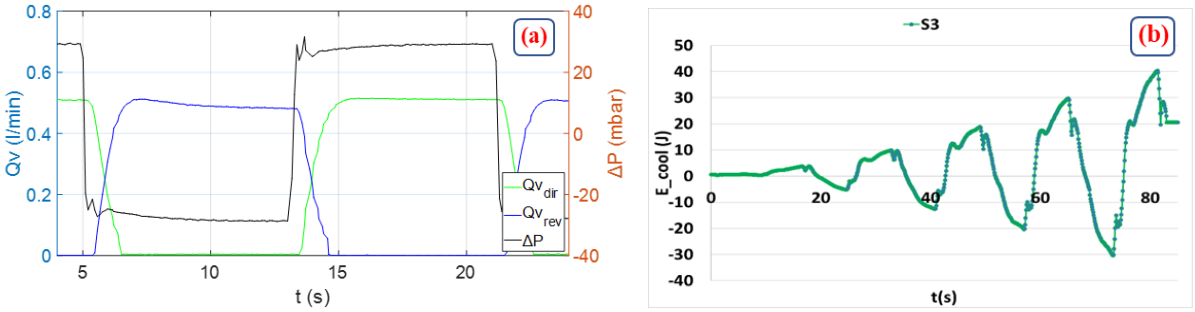

Figure 9: a) Pressure and flow signals during one cycle with S3 strategy; b) Energy transported by fluid flow under S3 strategy

Figure 9(b) illustrates the corresponding evolution of the energy exchanged between the coolant inlet and outlet (E_{cool}). An oscillatory behavior is observed throughout the startup phase. When the energy exchanged is positive, this indicates that the coolant fluid is absorbing heat, thus removing thermal energy from the cell. This suggests that part of the heated fluid becomes temporarily trapped within the stack volume and end zones, rather than circulating fully through the loop. These thermal oscillations reflect the dynamic redistribution of heat induced by the alternating flow strategy.

The cold start results using this strategy are presented in Figure 10(a). The average temperature rise for cells A, M, and K " γ " is 29.3°C. The standard deviation of the temperature rise "σ" is 2.6°C, indicating a significant improvement over the S1 strategy (7°C). Vertical temperature uniformity "δ" is better, measured at 1.9°C, implying a significant reduction compared with the S2 strategy (δ=6.3°C).

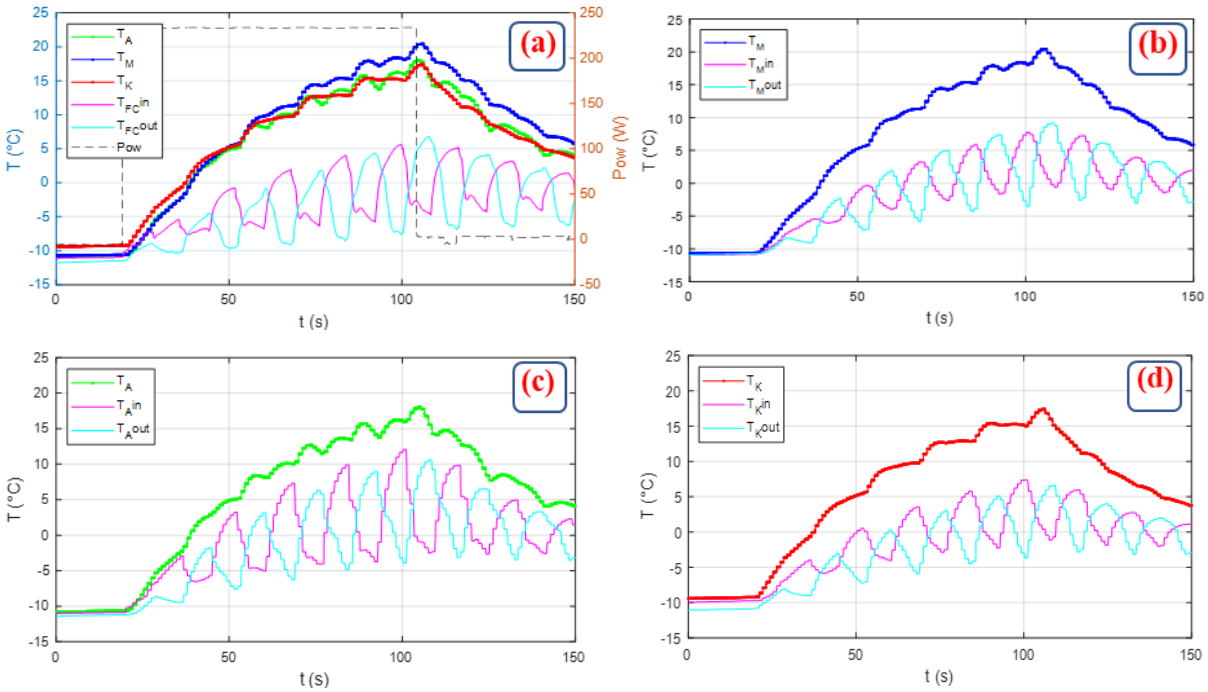

Figure 10: Alternating flow strategy "S3" (Qv =0.5 L/min; P=16s; DC=50%): (a) Temperatures of the three cells with fuel cell inlet and outlet; (b) Cell M with its inlet and outlet; (c) Cell A with its inlet and outlet; (d) Cell K with its inlet and outlet

Detailed analysis of inlet and outlet temperatures of the cooling plates (Figure 10 (b), (c), (d)) reveals that, during certain cold-start phases, these critical zones can exceed the freezing point under the alternating flow strategy, with fluctuations up to 5 °C. Flow reversal reinjects heated fluid into the stack, unlike S2, which introduces colder fluid at the inlet. This mechanism reduces cold spots and improves vertical thermal uniformity.

3.1.4 Alternating flow with stops strategy: S4

To optimize the alternating flow strategy regarding stack temperature rise, a phase in which the heat transfer fluid is halted inside the stack is intentionally introduced. This phase plays a crucial role in limiting heat exchange through forced convection.

The proposed strategy is also based on reversing the fluid flow direction through the stack. Still, after each movement in a given direction, a fluid stop phase is initiated within the stack. During this stop phase, solenoid valves redirect the fluid flow, allowing it to bypass the stack. This operation is confirmed by the variations in the pressure signal measured across the stack ($\Delta P = 0$) recorded during the process Figure 11 (a).The tested operating parameters—period of 16 s, duty cycle of 50%, stop ratio of 50%, and flow rate of 0.5 l/min—were selected to enable direct comparison with strategy S2 (same flow rate) and strategy S3 (same flow rate and period).

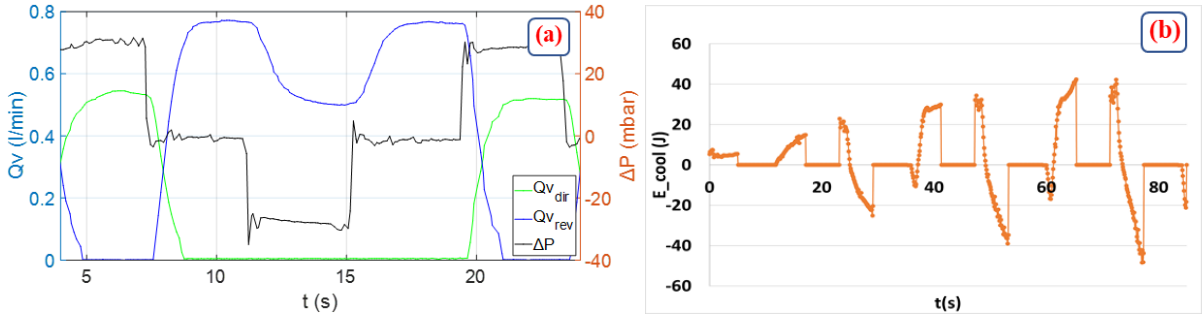

Figure 11: a) Pressure and flow signals during one cycle with S4 strategy; b) Energy transported by fluid flow under S3 strategy

After each stop, the fluid flows again in the opposite direction for the same duration of 4 s in this test. In the secondary circuit, the second flowmeter measures the flow rate observed when the coolant flows in the reverse direction as well as during the by-pass phase. When the fluid bypasses the stack, the flow rate measured in this circuit is higher than when the fluid passes through the stack. This difference is due to the change in pressure drop, as the pressure losses associated with the stack are absent in the bypass configuration. The key parameters of this strategy—namely the flow rate, period, duty cycle, and stop ratio—are fully adjustable and controllable. The profile of the energy transported by the movement of the fluid driven by the pump shows that after each fluid stop, the variation in thermal energy exchanged at the inlet and outlet of the stack changes sign, passing through zero, which indicates that the fluid heated by the stack enters and exits it in a periodic manner ((Figure 11 (b)).

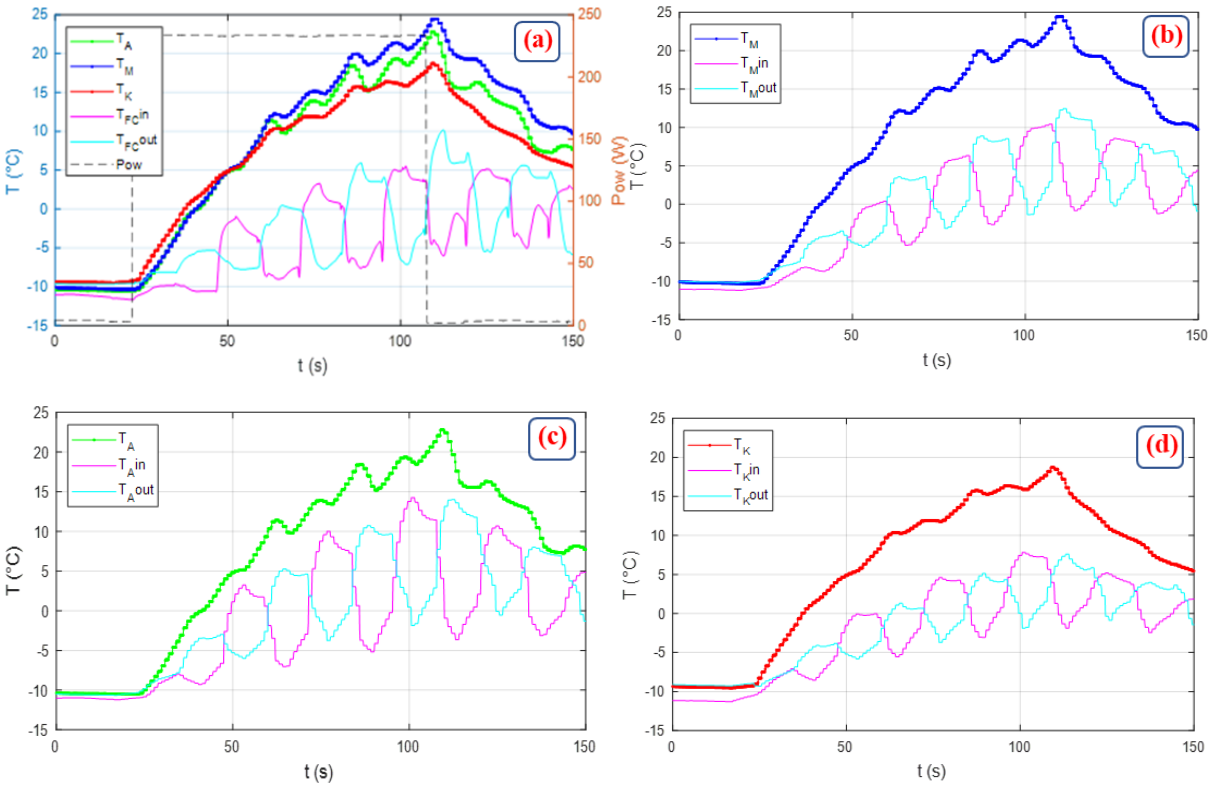

Figure 12: Alternating flow with stops strategy "S4" (Qv =0.5 L/min; P=16s; DC=50%; SR=50): (a) Temperatures of the three cells with fuel cell coolant inlet and outlet; (b) Cell M with its inlet and outlet; (c) Cell A with its inlet and outlet; (d) Cell K with its inlet

The cold start results using this strategy are illustrated in the Figure 12 (a). The maximum temperatures reached by cells TA, TM, and TK are 22.8 °C, 24.5 °C, and 18.7 °C, respectively. The standard deviation between cells A, M, and K is $\sigma = 2.9\,°C$. Additionally, the vertical temperature uniformity is evaluated at $\delta = 0.6\,°C$, indicating good homogeneity in vertical thermal distribution. The effect of the fluid stop phase

is reflected in a significant improvement in the average temperature rise of the stack (γ =32.3 °C). All cells successfully exit the sub-zero state by the end of the heating period (Figure 12 (b), (c), (d)).

3.1.5 Summary of the four Start-Up Strategies:

The main objective of this work is to present an experimental investigation of heating strategies to improve PEMFC cold start. The core contribution lies in the comparison of four different approaches, with Figure 13 (a) and Figure 13 (b) providing a comparative overview of their performance.

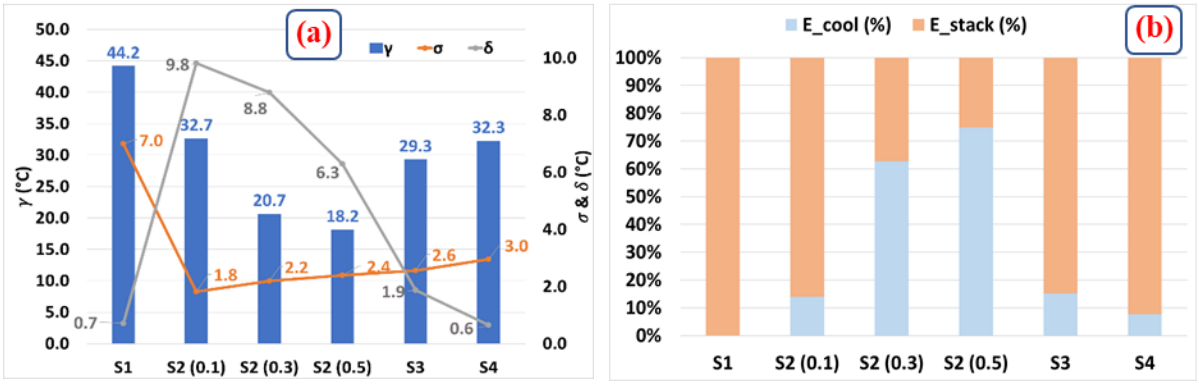

Figure 13: a) Comparative performance analysis of start-up strategies*; b) Heat transfer distribution for each tested strategy*

The first conventional strategy evaluated (S1) enabled rapid heating, reaching a temperature rise of 44.2 °C within 85 s. However, it also resulted in significant thermal non-uniformity, with a recorded standard deviation (σ) of 7 °C. In this configuration, central cells—better thermally insulated—heat primarily by conduction, whereas edge cells dissipate heat more rapidly. In real operating conditions, such overheating can lead to the rapid evaporation of water from the membrane [49] [46], causing a drastic increase in membrane resistance and, consequently, a voltage drop. This non-uniform temperature distribution results in heterogeneous degradation across the active surfaces of the cells. This reference test highlights the necessity of implementing heat transfer fluid circulation during the cold start phase to ensure thermal management and stack protection.

. Figure 13 (b) illustrates the distribution of energy losses across the system for each heating strategy. For the S1 strategy, it is assumed that the thermal energy supplied to the stack ($E_{surro} + E_{elec}$) is entirely transferred to the fuel cell (E_{stack}), contributing exclusively to its temperature rise.

The S2 strategy, based on unidirectional coolant flow, improved horizontal temperature uniformity, with standard deviations limited to 2.4 °C. However, it significantly reduced overall temperature rise due to forced convection: at a flow rate of 0.5 L/min, the temperature increase dropped by 60% compared to the S1 configuration. As shown in Figure 13 (b), the energy extracted by the coolant ranges from 14% to 75%, depending on the flow rate, which limits the heat retained within the stack. Consistent with previous findings [10], excessive coolant flow can remove too much thermal energy, potentially leading to startup failure. Moreover, this strategy induced vertical temperature gradients ranging from 6.3 °C to 9.8 °C, increasing the risk of ice formation at the bottom of the cells. During cold starts at −10 °C, inlet zones remained below −5 °C, favoring water freezing from electrochemical reactions. These conditions compromise membrane hydration and long-term durability, rendering this strategy unsuitable for reliable cold start operation.

The alternating flow strategy (S3) effectively addressed the limitations of the reference cases by reducing internal thermal gradients. The temperature standard deviation dropped from 7 °C (S1) to 2.6 °C, while achieving a higher temperature rise ($\gamma = 29.3\,°C$) than S2 ($\gamma = 18.2\,°C$) at the same flow rate (0.5 L/min). Heat losses were limited to 15%, as the heated fluid remained temporarily confined within the stack and its extremities, rather than being immediately evacuated through the cooling loop. These periodic oscillations raise the entire active surface above 0 °C at regular intervals, with local temperature variations up to 5 °C—thus enhancing thermal uniformity and reducing the risk of ice formation.

The improved strategy (S4) builds on the alternating flow approach (S3) by introducing a fluid stop phase between each directional change. This modification significantly enhanced heating performance. With a 16 s period, 50% duty cycle, 50% stop ratio, and a flow rate of 0.5 L/min, the temperature rise (γ) reached 73% of that achieved in S1, compared to 66% in S3. This improvement is attributed to reduced convective losses, which account for only 8% of the total thermal input. Thermally, this strategy significantly improved uniformity: the standard deviation (σ) across the three cells was reduced by 57% compared to S1, and the maximum temperature difference (δ) remained below 1 °C. Under −10 °C cold-start conditions, all cells exceeded the freezing threshold, enabling successful and uniform startup without compromising durability.

3.2 Effect of Coupled Velocity and Period on Cold Start Performance under Alternating Flow Conditions:

The results of the previous experimental campaign demonstrate the effectiveness of Strategy S4 in improving the cold start performance of the fuel cell. In the next part of this study, we present the results of a parametric experimental analysis aimed at investigating the impact of the coupling between the fluid flow rate (velocity) and the reciprocating period on the performance of this strategy

Two flow rates were selected: 0.1 L/min, corresponding to the minimum flow rate achievable by our experimental setup, and 0.5 L/min, representing the maximum permissible flow rate for our fuel cell prototype. In parallel, four reciprocating periods were investigated, ranging from 8 s to 32 s. This range was chosen based on the technical constraints of the test bench. It is also intended to cover the thermal dynamics of the stack. A period of 8 seconds implies a change in the state of the solenoid valves every 2 seconds, meaning a change of flow direction every 2 seconds, this is close to the operating limit of the solenoid valves for state switching. Conversely, the maximum period of 32 seconds was defined from the characteristic heating time of the stack (≈85 seconds). A duration of 32 seconds corresponds to the time required to observe a meaningful temperature rise. This choice ensures at least two complete alternating cycles within the heating phase, allowing the effect of longer periods on cold-start efficiency to be assessed.

Figure 14 groups the eight startup cases investigated. Graphs are arranged from top to bottom by increasing period, left column: minimum flow rate, right column: maximum flow rate. Figure 15 provides a summary of the associated performances.

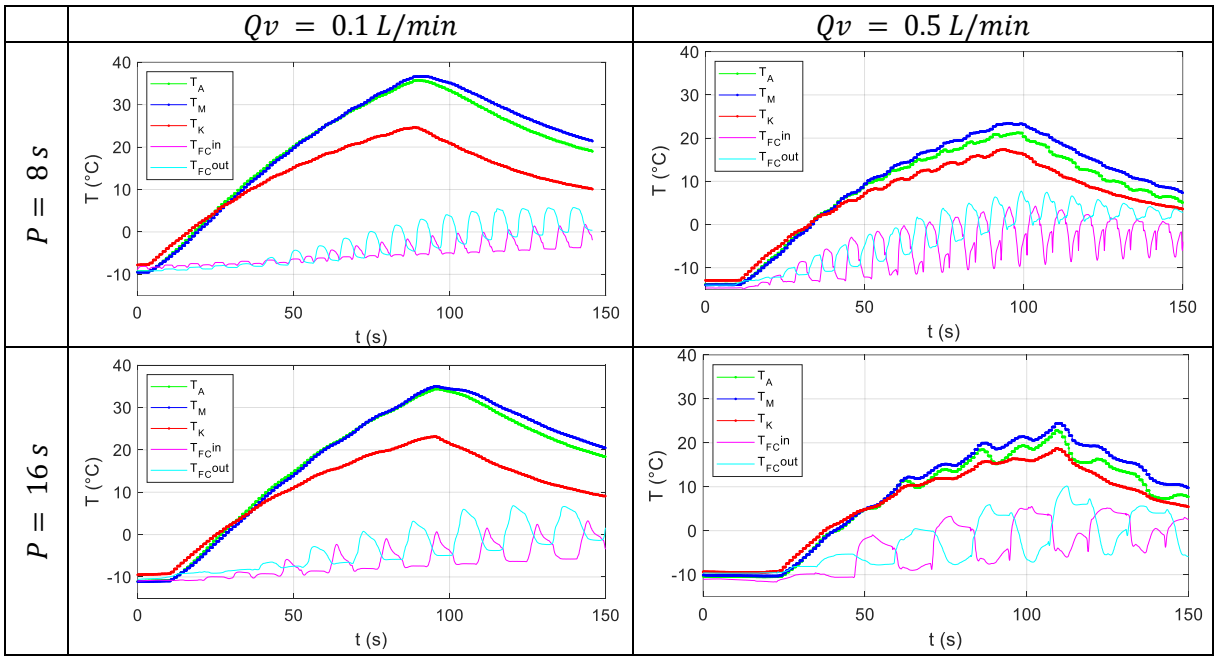

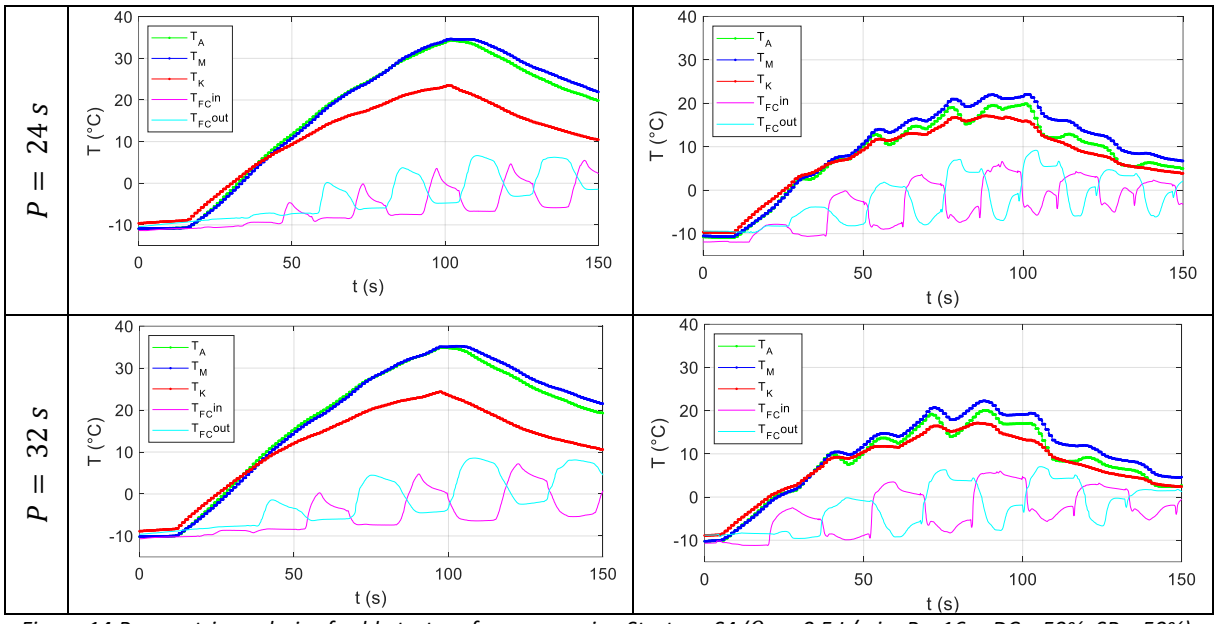

Figure 14:Parametric analysis of cold-start performance using Strategy S4 (Qv = 0.5 L/min; P = 16 s; DC = 50%; SR = 50%). Left: minimum flow rate; Right: maximum flow rate. Graphs are arranged in order of increasing period from top to bottom.

At low flow rates, the temperatures of the heating pads do not present oscillations and tend to be similar to those observed under the S1 strategy. However, the effect of the reciprocating period is noticeable at the inlet and outlet temperatures of the stack, indicating that the heated fluid remains trapped within the stack. For long periods, oscillations overlap, allowing the fluid to circulate. However, they have no significant impact on temperature rise due to the low flow rate, which remains nearly unchanged ($\gamma \approx 41\,°C$), (Figure 15).

At higher flow rates, oscillations appear in the heating pads and increase in amplitude with frequency. At short switching periods, the stack's inlet and outlet temperatures begin to show symmetry; however, the fluid does not have enough time (2 seconds) to fully reverse its direction. As the switching periods increase, oscillations become more pronounced, and the inlet and outlet temperatures become more symmetrical. This indicates that the heated fluid is extracted and then reinjected into the stack. This results in a temperature rise that decreases with longer period as the heat is distributed over a larger volume. The temperature rise varies from 29.5 °C to 34.5 °C (Figure 15) corresponding to 67% to 79% of the maximum temperature rise recorded during the S1 strategy.

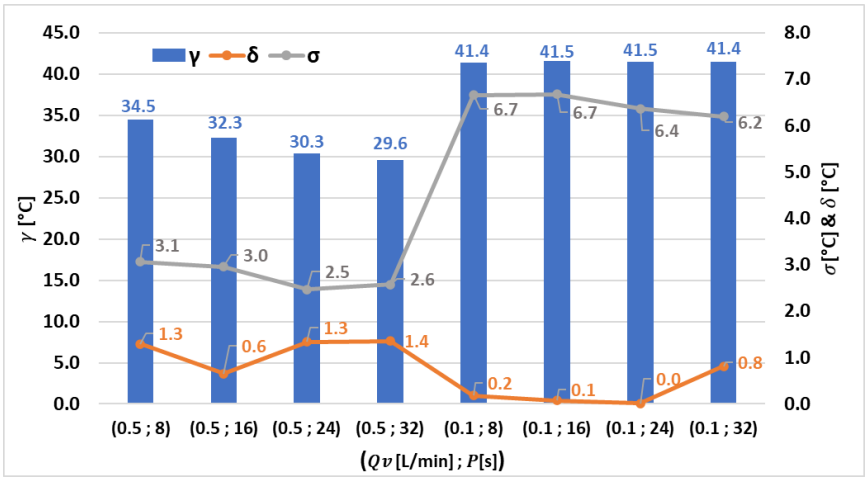

Figure 15: Performance Comparison of the Parametric Analysis According to $(Q_v; P)$ – S4 strategy

If the cooling fluid commutation time is too short, the cooling fluid that has absorbed the heat will not come out of the fuel cell; if this time is too long, the PEMFC temperature distribution will look like that of traditional unidirectional cooling. These observations are consistent with previous simulation-based

findings reported [40].
According to this analysis, the optimal coupling that provides a good compromise between the different performance indicators is $(Q_v; P) = (0.5\ L/min;\ 16s)$, with a stop ratio of 50% and a duty cycle of 50%. This strategy achieves:

- A temperature rise "γ" of 32.3 °C, corresponding to 73%of the maximum achievable increase,
- A 57% reduction in the standard deviation "σ" of the heating pad temperatures,
- An average vertical thermal uniformity "δ" below 1 °C at the cell level.

This optimal coupling is specific to this prototype and may not be directly transferable to other fuel cells under real operating conditions. However, the heating strategy—namely the alternating flow configuration including stops—can be a reference for adjusting optimal parameters in other systems during real-world operation.

3.3 Application Case (Non-uniform thermal power generation): Thermal Optimization of Peripheral Cells in the Stack Using Alternating Flows:

This section aims to highlight the benefit of alternating flows to increase the temperature of one of the cells located at the ends of the stack. It may be of significant matter as those cells are at higher risks of ice formation [10] [12]. Such ice formation may lead to an insufficient reactant supply. This supply deficit leads to limited heat generation, potentially resulting in a start-up failure of the affected cell. One of the key challenges in real fuel cell stacks is precisely this lack of reactant supply in the peripheral cells [11], which impacts current density and reduces heat production. This section explores how the alternating flow strategy can help support the underperforming cell by transferring heat generated from neighboring cells, thereby facilitating its temperature rise. To reproduce such a scenario, the heating power delivered by the pads is deliberately reduced for selected cells, simulating the behavior observed in real stacks when a cell operates under degraded conditions. As mentioned above (2.1), the heating power delivered by the pads is adjustable between the cells. Each cell effectively provides 100% of its nominal power, but in a discontinuous manner, so that the time-integrated energy corresponds to the desired reduced power.

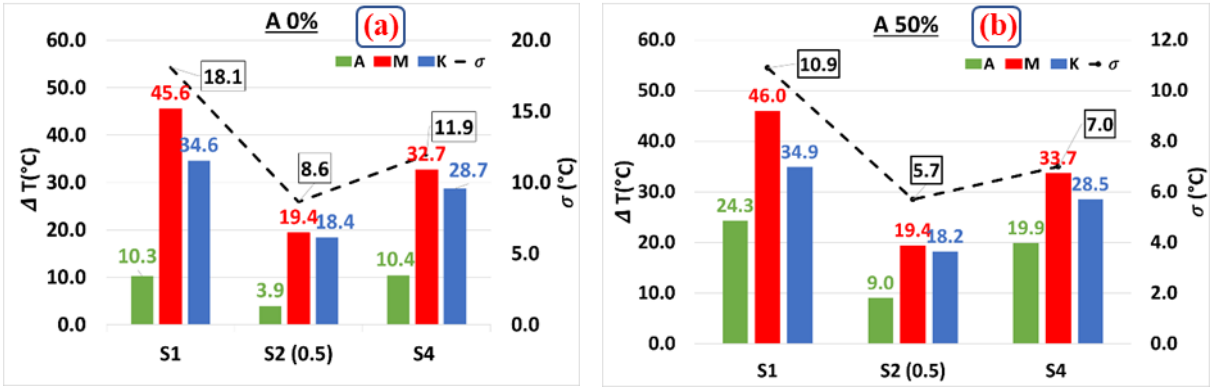

Figure 16: Performance Comparison: (a) Cell A generates no heat; (b) Cell A generates 50% of the nominal power

Two scenarios were investigated for the cell A suffers from insufficient reactant supply:

- In the first scenario, the target cell generates no heat (extreme case); it is denoted as A 0% (Figure 16(a)).
- In the second, it generates only 50% of its nominal power, while the other cells operate at full nominal power during the start-up phase, which is denoted as A 50% (Figure 16 (b)).

Three thermal management strategies were evaluated:

- S1: No-flow strategy
- S2: Unidirectional flow at 0.5 L/min
- S4: Alternating flow strategy with the following configuration: $Q_v = 0.5$ L/min; P = $16s$; $DC = 50\%$; $et\ RS = 50\%$.

Figure 16 provides a comparative overview of the performance of the three cells at the end of the startup phase at −10 °C when an extremity cell (Cell A) is deliberately underheated.
In the extreme case where no heating is applied to Cell A (Figure 14a), only strategies S1 and S4 enable its temperature to increase by more than 10 °C and reach 0 °C, thereby exiting the frozen state. In contrast, the unidirectional flow strategy (S2) fails to achieve this target. Furthermore, thermal uniformity across the

stack is significantly improved with strategy S4, showing a reduced standard deviation ($\sigma = 11.9\,°C$) compared to S1 ($\sigma = 18.1\,°C$). The temperature rise of Cell A under S4 is comparable to that obtained with S1, but the underlying mechanisms differ: in S1, heat transfer is mainly limited to conduction, whereas in S4, the alternating flow promotes both conduction and forced convection. This behavior facilitates heat accumulation within the stack volume and enables thermal energy transfer from neighboring cells (K and M) to the underperforming Cell A. In the second scenario (partial heating, Figure 16(b)), strategy S4 again results in an intermediate temperature rise relative to the two reference strategies, while further enhancing thermal uniformity ($\sigma = 7°C$). This further confirms that alternating flow fosters intra-stack heat accumulation and promotes effective thermal energy transfer from adjacent cells to the underperforming cell.

In conclusion, we observe that using an alternating flow strategy has a specific positive impact on the thermal behavior of end cells during cold start. By enabling heat transfer from neighboring cells, it helps support the underperforming cell and facilitates its temperature rise. This effect occurs because the heated coolant volume remains trapped within the stack during alternation, unlike in the unidirectional strategy where it is continuously evacuated.

3.4 Adaptive Thermal Management Strategy: S5

In the previous paragraphs, the strategies were applied under constant conditions (e.g., fixed flow rate and period) to facilitate their analysis and comparisons with each other. However, in real operation, dynamic control of the coolant circuit is needed. Therefore, an adaptive switching strategy (S5) is proposed to improve thermal homogeneity during cold start. This strategy combines the benefits of the S1 approach, known for limiting heat transfer and thus enabling rapid temperature rise, with those of alternating circulation, which helps reduce thermal gradients within the stack. This approach relies on continuous inspection of the temperature field within the fuel cell stack. As shown in Figure 17(C), once the temperature dispersion between cells exceeds a defined threshold—set empirically at 4 °C in this study to indicate the onset of significant imbalance—that could affect system performance. In this case, the standard strategy (S1), typically based on no-flow, is replaced by an alternating flow strategy. The goal is to accelerate the cold start process without compromising thermal balance across the stack. In the following, we present the results of this dynamic control approach.

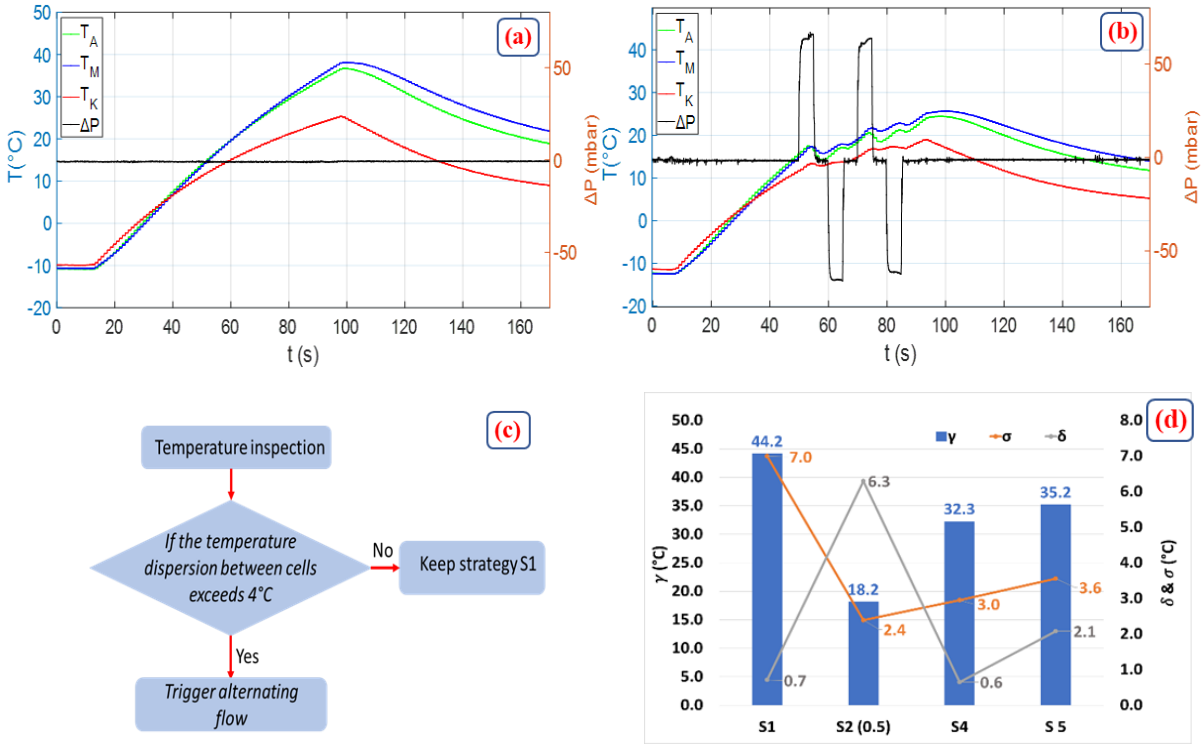

Figure 17:a) Cold start experiments using Strategy S1, b) Cold start experiments using S5, c) Schematic of the control strategy S5, d) Performance Comparison Between adaptive S5 and Reference Thermal Management Strategies

Figure 17 (a) shows the temperature evolution of the three heating pads under Strategy S1. On the secondary axis, the ΔP signal remains zero, indicating the absence of flow circulation. As previously discussed, this strategy leads to a significant temperature standard deviation between the cells σ, reaching 7 °C.

Figure 17 (b) illustrates the results obtained with the adaptive strategy S5. Once the temperature difference between the cells exceeds a defined threshold, alternating flow circulation is activated. This is evidenced by the ΔP signal, which oscillates periodically, reflecting the reversal of flow direction through the fuel cell stack. These changes are also visible in the corresponding temperature oscillations observed at that moment. In real operation – with electrochemical activity - where the individual cell's temperature is not known, the trigger could instead be based on inter-cell voltage deviations. Although the present study adopts a pragmatic temperature difference of 4 °C, this value can be further optimized with larger datasets or replaced by electrochemical indicators more accessible in real stacks.

Figure 17 (d) presents the performance indicators for the proposed adaptive strategy alongside those of three reference strategies. The adaptive strategy demonstrates a significantly higher temperature rise γ (35.2 °C) than Strategies S2 (18.2 °C) and S4 (32.3 °C), while maintaining temperature uniformity σ (3.6 °C) within an acceptable value.

From a scientific perspective, this strategy represents a novel step beyond conventional fixed control laws. Previous studies have either focused on maximizing heat production through various load-control strategies or on improving spatial uniformity via alternating reactant supply. They have rarely considered combining these approaches within a unified thermal management strategy. The adaptive strategy shows that PEMFC thermal management can be optimized through dynamic control of flow regimes, rather than relying solely on hardware modifications or external heaters.

From a practical perspective, this approach is also scalable and low-cost, since it relies only on simple modifications of flow control laws within an existing fluid management system. This makes it highly attractive for integration into automotive applications, where robustness, energy efficiency, and limited auxiliary consumption are key factors.

In summary, the adaptive flow strategy not only enhances thermal performance during sub-freezing PEMFC start-ups but also provides a generalizable framework for smart thermal management.

4. Conclusion:

This study demonstrates the effectiveness of alternating flow strategies in improving cold-start performance of PEMFCs by accelerating stack heating, enhancing thermal uniformity, and facilitating inter-cell heat transfer. This approach directly addresses the limitations of conventional passive strategies, particularly their difficulty in maintaining thermal balance during cold start.

First, the limitations of conventional methods were first identified:

- S1 (no-flow): achieved fast heating, high vertical temperature homogeneity within the cells, but produced large temperature differences between cells resulting in poor horizontal uniformity.
- S2 (unidirectional flow): achieved reduced heating, high vertical temperature homogeneity, and low horizontal temperature uniformity,

Three novel alternating flow strategies were then evaluated as passive heating solutions without external energy supply:

- S3 (alternating flow): demonstrated an improved heating compared to unidirectional flow while maintaining both cell-level and stack-level homogeneity by retaining the generated heat within the stack. Flow oscillations allowed all cells to periodically exceed the freezing point (up to 5 °C variation).

- S4 (alternating flow with stop phase): further improved S3 by introducing a fluid stop period. It achieved 73% of the temperature rise while enhancing horizontal uniformity by ~57% observed in S1. Vertical uniformity was preserved, and all cells successfully exited the sub-zero regime at –10 °C, ensuring safe and reliable startup.

  A parametric study highlighted the importance of optimizing the alternating period: when too short it prevents heat evacuation, whereas when too long it tends to unidirectional flow behavior. Alternating flows in cold start are especially effective for edge cells. Indeed, they make it possible to compensate for a possible drop in heat production due to ice formation by the circulation of the liquid heated by the other cells.

- Based on these findings, an adaptive dynamic thermal management strategy (S5) is proposed. By dynamically switching between heating modes according to internal thermal monitoring, this approach can accelerate cold start while preserving stack homogeneity. It opens new perspectives for coupled electro–thermal–fluidic control, where flow parameters are adjusted in real time to both voltage and temperature. This offers a promising pathway for practical PEMFC implementation.

Alternating flow strategies provide a cost-effective passive heating strategy, while still improving stack heating and thermal uniformity. Their implementation through standard automotive components makes the concept scalable to larger stacks, though careful optimization is needed to address amplified thermal gradients, flow distribution, and component sizing.

While this study offers valuable insights using a thermal emulator, its main limitation is the use of a constant artificial heat source. Future work will focus on real PEMFC stacks operating under realistic conditions, including water production, ice formation, and degradation. Tests on larger stacks will also be conducted to better capture full-scale thermal dynamics and heterogeneities.

Declaration of competing interest:

The authors declare that they have no known competing financial interests or personal relationships that could have appeared to influence the work reported in this paper.

Acknowledgements:

This work has been supported by EIPHI Graduate School (contract ANR-17-EURE-0002), Region Bourgogne-Franche-Comté.

[1] N. A. A. Qasem, "A recent overview of proton exchange membrane fuel cells: Fundamentals, applications, and advances," *Applied Thermal Engineering*, vol. 252, p. 123746, Sep. 2024, doi: 10.1016/j.applthermaleng.2024.123746.

[2] K. Han, B. K. Hong, S. H. Kim, B. K. Ahn, and T. W. Lim, "Influence of anisotropic bending stiffness of gas diffusion layers on the degradation behavior of polymer electrolyte membrane fuel cells under freezing conditions," *International Journal of Hydrogen Energy*, vol. 36, no. 19, pp. 12452–12464, 2011, doi: https://doi.org/10.1016/j.ijhydene.2011.06.109.

[3] G. Montaner Ríos, J. Schirmer, C. Gentner, and J. Kallo, "Efficient thermal management strategies for cold starts of a proton exchange membrane fuel cell system," *Applied Energy*, vol. 279, p. 115813, Dec. 2020, doi: 10.1016/j.apenergy.2020.115813.

[4] F. Jiang and C.-Y. Wang, "Potentiostatic Start-Up of PEMFCs from Subzero Temperatures," *Journal of The Electrochemical Society*, vol. 155, no. 7, p. B743, May 2008, doi: 10.1149/1.2927381.

[5] "DOE Technical Targets for Fuel Cell Systems and Stacks for Transportation Applications." Hydrogen and Fuel Cell Technologies Office. [Online]. Available: https://www.energy.gov/eere/fuelcells/doe-technical-targets-fuel-cell-systems-and-stacks-transportation-applications

[6] "Current Status of Hyundai's FCEV Development. CITA 2019." HYUNDAI MOTOR GROUP. [Online]. Available: https://www.hyundainews.com/assets/documents/original/31505-20180220CurrentStatusofHyundaiFCEVDevelopment1.pdf

[7] M. Oszcipok, D. Riemann, U. Kronenwett, M. Kreideweis, and M. Zedda, "Statistic analysis of operational influences on the cold start behaviour of PEM fuel cells," *Journal of Power Sources*, vol. 145, no. 2, pp. 407–415, Aug. 2005, doi: 10.1016/j.jpowsour.2005.02.058.

[8] E. L. Thompson, J. Jorne, W. Gu, and H. A. Gasteiger, "PEM Fuel Cell Operation at − 20 ° C . II. Ice Formation Dynamics, Current Distribution, and Voltage Losses within Electrodes," *Journal of The Electrochemical Society*, vol. 155, no. 9, p. B887, Jul. 2008, doi: 10.1149/1.2943203.

[9] Y. Tabe, K. Yamada, R. Ichikawa, Y. Aoyama, K. Suzuki, and T. Chikahisa, "Ice Formation Processes in PEM Fuel Cell Catalyst Layers during Cold Startup Analyzed by Cryo-SEM," *J. Electrochem. Soc.*, vol. 163, no. 10, pp. F1139–F1145, 2016, doi: 10.1149/2.1321609jes.

[10] P. Lv *et al.*, "The voltage uniformity analysis of high-power proton exchange membrane fuel cell stack during cold start," *Applied Energy*, vol. 393, p. 125999, Sep. 2025, doi: 10.1016/j.apenergy.2025.125999.

[11] R. Lin *et al.*, “Consistency analysis of polymer electrolyte membrane fuel cell stack during cold start,” *Applied Energy*, vol. 241, pp. 420–432, May 2019, doi: 10.1016/j.apenergy.2019.03.091.
[12] X. Wan *et al.*, “End Plate Effects on the Performance of PEMFCs During Cold Start Process,” *J. Electrochem. Soc.*, vol. 168, no. 12, p. 124510, Dec. 2021, doi: 10.1149/1945-7111/ac4377.
[13] F. Wang, H. Zhang, P. Ming, D. Yang, B. Li, and C. Zhang, “Experimental study on rapid cold start-up performance of PEMFC system,” *International Journal of Hydrogen Energy*, vol. 48, no. 57, pp. 21898–21907, Jul. 2023, doi: 10.1016/j.ijhydene.2023.01.364.
[14] Y. Shan and S.-Y. Choe, “Modeling and simulation of a PEM fuel cell stack considering temperature effects,” *Journal of Power Sources*, vol. 158, no. 1, pp. 274–286, Jul. 2006, doi: 10.1016/j.jpowsour.2005.09.053.
[15] R. Lin, Y. Weng, Y. Li, X. Lin, S. Xu, and J. Ma, “Internal behavior of segmented fuel cell during cold start,” *International Journal of Hydrogen Energy*, vol. 39, no. 28, pp. 16025–16035, Sep. 2014, doi: 10.1016/j.ijhydene.2013.12.083.
[16] R. Lin, Y. S. Ren, X. W. Lin, Z. H. Jiang, Z. Yang, and Y. T. Chang, “Investigation of the internal behavior in segmented PEMFCs of different flow fields during cold start process,” *Energy*, vol. 123, pp. 367–377, Mar. 2017, doi: 10.1016/j.energy.2017.01.138.
[17] P. Ren, P. Pei, Y. Li, Z. Wu, D. Chen, and S. Huang, “Degradation mechanisms of proton exchange membrane fuel cell under typical automotive operating conditions,” *Progress in Energy and Combustion Science*, vol. 80, p. 100859, Sep. 2020, doi: 10.1016/j.pecs.2020.100859.
[18] X. Yang, J. Sun, X. Meng, S. Sun, and Z. Shao, “Cold start degradation of proton exchange membrane fuel cell: Dynamic and mechanism,” *Chemical Engineering Journal*, vol. 455, p. 140823, Jan. 2023, doi: 10.1016/j.cej.2022.140823.
[19] X. Yang, J. Sun, S. Sun, and Z. Shao, “An efficient cold start strategy for proton exchange membrane fuel cell stacks,” *Journal of Power Sources*, vol. 542, p. 231492, Sep. 2022, doi: 10.1016/j.jpowsour.2022.231492.
[20] D. Zhong *et al.*, “Low temperature durability and consistency analysis of proton exchange membrane fuel cell stack based on comprehensive characterizations,” *Applied Energy*, vol. 264, p. 114626, Apr. 2020, doi: 10.1016/j.apenergy.2020.114626.
[21] H. Su, H. Xu, L. Wang, Z. Liu, and L. Xie, “A review on thermal management strategy for liquid-cooling proton exchange membrane fuel cells: Temperature regulation and cold start,” *Applied Energy*, vol. 393, p. 126142, Sep. 2025, doi: 10.1016/j.apenergy.2025.126142.
[22] A. Amamou, M. Kandidayeni, L. Boulon, and S. Kelouwani, “Real time adaptive efficient cold start strategy for proton exchange membrane fuel cells,” *Applied Energy*, vol. 216, pp. 21–30, Apr. 2018, doi: 10.1016/j.apenergy.2018.02.071.
[23] W. Li, J. Yang, C. Du, J. Zhao, Q. Xin, and F. Yan, “Cold Start Performance Analysis of Pemfc with Different Assisted Heating Strategies,” 2025. doi: 10.2139/ssrn.5151460.
[24] A. A. Amamou, S. Kelouwani, L. Boulon, and K. Agbossou, “A Comprehensive Review of Solutions and Strategies for Cold Start of Automotive Proton Exchange Membrane Fuel Cells,” *IEEE Access*, vol. 4, pp. 4989–5002, 2016, doi: 10.1109/ACCESS.2016.2597058.
[25] T. Zhao and P. Cheng, “Heat Transfer in oscillatory flows, annual review of heat transfer,” in *Annual review of heat transfer*, vol. 9, 1998.
[26] D. K. Sharma and A. Prabhakar, “A review on air cooled and air centric hybrid thermal management techniques for Li-ion battery packs in electric vehicles,” *Journal of Energy Storage*, vol. 41, p. 102885, Sep. 2021, doi: 10.1016/j.est.2021.102885.
[27] R. Mahamud and C. Park, “Reciprocating air flow for Li-ion battery thermal management to improve temperature uniformity,” *Journal of Power Sources*, vol. 196, no. 13, pp. 5685–5696, Jul. 2011, doi: 10.1016/j.jpowsour.2011.02.076.
[28] X. Lin *et al.*, “Parameterization and observability analysis of scalable battery clusters for onboard thermal management,” *Oil & Gas Science and Technology–Revue d’IFP Energies nouvelles*, vol. 68, no. 1, pp. 165–178, 2013.
[29] C. Park and A. K. Jaura, “Dynamic thermal model of li-ion battery for predictive behavior in hybrid and fuel cell vehicles,” SAE Technical Paper, 2003.
[30] Z. Jiang, H. Li, Z. Sun, and Z. Qu, “Experimental study on 18650 lithium-ion battery-pack cooling system composed of heat pipe and reciprocating air flow with water mist,” *International Journal of Heat and Mass Transfer*, vol. 222, p. 125171, 2024, doi: https://doi.org/10.1016/j.ijheatmasstransfer.2024.125171.
[31] W. Zeng, C. Ma, S. Hu, S. Li, and Y. Zhang, “The performance investigation and optimization of reciprocating flow applied for liquid-cooling-based battery thermal management system,” *Energy Conversion and Management*, vol. 292, p. 117378, 2023, doi: https://doi.org/10.1016/j.enconman.2023.117378.

[32] K. Yu, X. Yang, Y. Cheng, and C. Li, “Thermal analysis and two-directional air flow thermal management for lithium-ion battery pack,” *Journal of Power Sources*, vol. 270, pp. 193–200, 2014, doi: https://doi.org/10.1016/j.jpowsour.2014.07.086.
[33] F. He and L. Ma, “Thermal management of batteries employing active temperature control and reciprocating cooling flow,” *International Journal of Heat and Mass Transfer*, vol. 83, pp. 164–172, 2015, doi: https://doi.org/10.1016/j.ijheatmasstransfer.2014.11.079.
[34] C. Park and A. K. Jaura, “Reciprocating battery cooling for hybrid and fuel cell vehicles,” *ASME International Mechanical Engineering Congress and Exposition*, pp. 425–430, 2003.
[35] Y. Liu, C. Ouyang, Q. Jiang, and B. Liang, “Design and parametric optimization of thermal management of lithium-ion battery module with reciprocating air-flow,” *Journal of central south university*, vol. 22, no. 10, pp. 3970–3976, 2015.
[36] Y.-W. Wang, J.-M. Jiang, Y.-H. Chung, W.-C. Chen, and C.-M. Shu, “Forced-air cooling system for large-scale lithium-ion battery modules during charge and discharge processes,” *Journal of Thermal Analysis and Calorimetry*, vol. 135, pp. 2891–2901, 2019.
[37] M. D. Alam, M. Almas, S. Soleimanikutanaei, and Y. Cao, “Experimental and Analytical Studies of Reciprocating Flow Heat Transfer in a Reciprocating Loop Device for Electronics Cooling,” *Fluids*, vol. 7, no. 4, 2022, doi: 10.3390/fluids7040132.
[38] S. Bégot, F. Harel, V. Lepiller, and W. Hafsa Saidouni, “A new cooling circuit and its control strategies for the thermal management of PEMFC in rapid startup application,” *International Journal of Hydrogen Energy*, vol. 48, no. 34, pp. 12826–12843, Apr. 2023, doi: 10.1016/j.ijhydene.2022.12.166.
[39] S. Begot *et al.*, “Système de refroidissement pour pile à combustible,” WO2012104553A1
[40] H. Shen *et al.*, “Effect of the cooling water flow direction on the performance of PEMFCs,” *International Journal of Heat and Mass Transfer*, vol. 189, p. 122303, Jun. 2022, doi: 10.1016/j.ijheatmasstransfer.2021.122303.
[41] P. He *et al.*, “Experimental investigation on the impact of ambient temperature and current load rate on the cold start behavior of a short PEMFC stack,” *Applied Energy*, vol. 396, p. 126317, Oct. 2025, doi: 10.1016/j.apenergy.2025.126317.
[42] W. Zhu, Y. Wang, S. Gao, F. He, C. Li, and Y. Wang, “Study on cold start of fuel cell stack combined with liquid heating and fuel cell self-starting,” *Case Studies in Thermal Engineering*, vol. 60, p. 104814, Aug. 2024, doi: 10.1016/j.csite.2024.104814.
[43] A.-U.-H. Najmi, V. S. Sudheendra Karur, T. Esch, and B. Shabani, “Efficient cold start of Proton exchange membrane fuel cells using a waste heat recovery system for coolant preheating,” *Energy Conversion and Management*, vol. 344, p. 120273, Nov. 2025, doi: 10.1016/j.enconman.2025.120273.
[44] Q. Cao *et al.*, “A novel thermal management for PEM fuel cell stack combining phase change materials with liquid cooling under low temperature condition,” *Applied Thermal Engineering*, vol. 238, p. 121949, Feb. 2024, doi: 10.1016/j.applthermaleng.2023.121949.
[45] X. Deng *et al.*, “Cold start of PEMFCs based on adaptive strategies: A comprehensive review,” *International Journal of Hydrogen Energy*, vol. 100, pp. 1120–1134, Jan. 2025, doi: 10.1016/j.ijhydene.2024.12.445.
[46] B. M. Sudaroli and V. Vasanthkumar, “Thermal behavior and performance evaluation of a 5-cell PEMFC stack operating with and without active cooling,” *Applied Thermal Engineering*, p. 128627, Oct. 2025, doi: 10.1016/j.applthermaleng.2025.128627.
[47] P. Chippar and H. Ju, “Evaluating cold-start behaviors of end and intermediate cells in a polymer electrolyte fuel cell (PEFC) stack,” *Solid State Ionics*, vol. 225, pp. 85–91, Oct. 2012, doi: 10.1016/j.ssi.2012.02.038.
[48] X. Yang, J. Sun, S. Sun, H. Yu, and Z. Shao, “Study on the temperature distribution and its effect on self-start of large-area proton exchange membrane fuel cells at subzero temperatures,” *Electrochimica Acta*, vol. 396, p. 139183, Nov. 2021, doi: 10.1016/j.electacta.2021.139183.
[49] R. Eckl, W. Zehtner, C. Leu, and U. Wagner, “Experimental analysis of water management in a self-humidifying polymer electrolyte fuel cell stack,” *Journal of Power Sources*, vol. 138, no. 1–2, pp. 137–144, Nov. 2004, doi: 10.1016/j.jpowsour.2004.06.042.